

PDCS: A Primal-Dual Large-Scale Conic Programming Solver with GPU Enhancements

Zhenwei Lin* Zikai Xiong[†] Dongdong Ge[‡] Yinyu Ye[§]

May 1, 2025

Abstract

In this paper, we introduce the **Primal-Dual Conic Programming Solver (PDCS)**, a large-scale conic programming solver with GPU enhancements. Problems that PDCS currently supports include linear programs, second-order cone programs, convex quadratic programs, and exponential cone programs. PDCS achieves scalability to large-scale problems by leveraging sparse matrix-vector multiplication as its core computational operation, which is both memory-efficient and well-suited for GPU acceleration. The solver is based on the restarted primal-dual hybrid gradient method but further incorporates several enhancements, including adaptive reflected Halpern restarts, adaptive step-size selection, adaptive weight adjustment, and diagonal rescaling. Additionally, PDCS employs a bijection-based method to compute projections onto rescaled cones. Furthermore, cuPDCS is a GPU implementation of PDCS and it implements customized computational schemes that utilize different levels of GPU architecture to handle cones of different types and sizes. Numerical experiments demonstrate that cuPDCS is generally more efficient than state-of-the-art commercial solvers and other first-order methods on large-scale conic program applications, including Fisher market equilibrium problems, Lasso regression, and multi-period portfolio optimization. Furthermore, cuPDCS also exhibits better scalability, efficiency, and robustness compared to other first-order methods on the conic program benchmark dataset CBLIB. These advantages are more pronounced in large-scale, lower-accuracy settings.

1 Introduction

Convex conic programming aims to find an optimal solution that minimizes (or maximizes) a linear objective function while remaining within the feasible region defined by the intersection of a linear subspace and a convex cone. Many important real-world decision-making models can be formulated

*School of Industrial Engineering, Purdue University, West Lafayette, IN 47907, USA. lin2193@purdue.edu

[†]Operations Research Center, MIT, Cambridge, MA 02139, USA. zikai@mit.edu (Corresponding author)

[‡]Antai School of Economics and Management, Shanghai Jiao Tong University, Shanghai, China. ddge@sjtu.edu.cn

[§]Department of Management Science and Engineering, Stanford University, Stanford, CA 94305, USA. yyye@stanford.edu

as conic programs. Typical examples include, but are not limited to, linear programs (LPs), second-order cone programs (SOCPs), semidefinite programs (SDPs), and exponential cone programs. Conic programs have extensive applications across numerous fields, including economics (see, e.g., [26, 55]), transportation (see, e.g., [11]), energy (see, e.g., [13]), healthcare (see, e.g., [45, 4]), finance (see, e.g., [53]), manufacturing (see, e.g., [8, 31]), computer science (see, e.g., [15]), and medicine (see, e.g., [58]), among many others.

Since the mid-20th century, the development of efficient solution methods for conic programs has been a central topic in the optimization community, with significant efforts focused on improving both computational speed and scalability. Nearly all existing general-purpose solvers for conic programs are based on either the simplex method (for LP problems) or the barrier method (also known as the interior-point method). These methods are widely implemented in most commercial optimization solvers.

Despite their effectiveness for solving moderate-sized instances, both the simplex and barrier methods become impractical for large-scale problems. The primary bottleneck is their reliance on matrix factorizations—such as LU factorization for the simplex method and Cholesky factorization for the interior-point method—which are required to repeatedly solve linear systems at each iteration. The computational cost of matrix factorizations grows superlinearly with problem size, measured in terms of the number of decision variables, constraints, or nonzero entries in the problem data. This limitation arises from two main challenges. First, matrix factorizations are highly memory-intensive, and even sparse matrices can produce dense factors, making storage and computation prohibitive. Second, these factorization-based methods are inherently sequential, limiting their suitability for modern parallel and distributed computing architectures, such as graphics processing units (GPUs). Due to these challenges, early efforts to leverage GPUs in commercial solvers have largely been unsuccessful [25].

Meanwhile, outside of conic solver development, GPU-based parallel computing has emerged as a powerful tool for scaling up modern computational applications, most notably in the training of large-scale deep learning models. This contrast highlights the need for alternative conic program solvers that better align with modern high-performance computing architectures.

To better harness the power of GPUs and more efficiently solve large-scale conic programs, a matrix-free first-order method (FOM) is a promising choice. A matrix-free FOM addresses the two challenges mentioned above by eliminating the need for matrix factorizations and instead relying on more computationally efficient operations such as matrix-vector products. These operations are well-suited for GPU acceleration.

In the context of these developments, this paper aims to develop a matrix-free FOM-based solver for solving large-scale conic programs. The solver we develop in this paper is called the “Primal-Dual Conic Programming Solver” (PDCS) because it is based on the primal-dual hybrid gradient method (PDHG). PDCS is designed to solve conic programs where the feasible region consists of Cartesian products of zero cones, nonnegative cones, second-order cones, and exponential cones. We also develop a GPU-enhanced implementation of PDCS that is called cuPDCS. As one might expect,

for small-scale problems, the interior-point methods in commercial solvers are consistently better than first-order methods (including PDCS) in efficiency and robustness. However, our experimental results demonstrate that cuPDCS achieves the following advantages:

1. cuPDCS is generally more efficient than state-of-the-art commercial solvers and other existing first-order methods on large-scale conic program applications.
2. cuPDCS exhibits better scalability, efficiency, and robustness compared to other first-order methods on the small-scale conic program benchmark dataset CBLIB.

Furthermore, the above two advantages are more pronounced in large-scale, lower-accuracy settings. The PDHG algorithm and the associated practical enhancements used in our PDCS do not need any matrix factorizations. As a result, the computational bottleneck of PDCS is performing (sparse) matrix-vector products when computing gradients. Thanks to recent advancements in GPU hardware and software optimization, sparse matrix-vector multiplication (SpMV) has been extensively optimized for GPUs, making cuPDCS orders of magnitude faster than its CPU-based counterparts.

Recently, PDHG has shown promising progress in solving large-scale linear programs and exploiting GPU acceleration. PDHG is used to directly solve the saddle-point formulation of LP [2]. Several large-scale LP solvers have been developed based on PDHG in combination with effective heuristics. Notable implementations include PDL for CPUs [1] and cuPDL [40] along with its C-language version cuPDL-C [44] for GPUs. [40, 44] have shown that GPU-based implementations of PDHG already outperform classical methods implemented in commercial solvers on a significant number of problem instances. As a result, PDHG has been integrated as a new algorithm for LP in COPT [23], Xpress [7], and Gurobi [51]. Additionally, it has been incorporated into Google OR-Tools [1], HiGHS [23], and NVIDIA cuOpt [20].

As for the general conic programs, [63] has established that PDHG (with restarts) can also solve conic programs beyond LPs. However, no practical PDHG-based solver has been developed for conic programs, and it remains unknown whether GPUs can provide similar computational advantages for general-purpose conic solvers.

To better unleash the potential of PDHG and utilize the efficiency of GPU, there are several enhancements implemented in PDCS (and cuPDCS). These enhancements go beyond a straightforward GPU implementation and involve algorithmic improvements, specialized projection methods, and customized parallelism strategies: (a) Algorithmic improvements: PDCS is based on a variant of PDHG that integrates several effective enhancements, including adaptive Halpern restarts, diagonal rescaling, and adaptive step-size selection. Some of these heuristics have been proven effective in the PDHG-based LP solver PDL [1]. (b) Specialized projection methods: PDHG requires frequent Euclidean projections onto the underlying cones. While efficient projection methods exist for many common cones, such as nonnegative cones, second-order cones, and exponential cones, projections onto rescaled cones (after applying diagonal rescaling) can become nontrivial. PDCS addresses this by employing bijection-based algorithms. These methods maintain computational complexity comparable to that of projecting onto the original, unrescaled cones. (c) Customized parallelism strategies: Unlike LPs, which involve only nonnegative cones, the underlying cones in general conic

programs are often more complex, consisting of Cartesian products of multiple cones of different types and sizes. To better leverage GPU parallelism and accommodate the varying structure of the cones, cuPDCS implements customized computational schemes that utilize different levels of GPU architecture to handle different cones of different types and sizes.

It should be mentioned that PDCS also applies to general semidefinite programming (SDP) problems but it requires conducting a Euclidean projection onto the semidefinite cone in each iteration, whose cost grows superlinearly with respect to the problem dimension. For these SDP problems, recent works [30, 29] propose a less expensive GPU-based first-order solver cuLoRADS that is based on the alternating direction method of multipliers (ADMM) and the Burer-Montonio method. It does not require projections onto the cone and exhibits better performance than commercial solvers in solving many large-scale SDP problem instances. In contrast, our PDCS focuses on cones other than semidefinite cones.

We conducted computational experiments to evaluate the efficiency, stability, and scalability of cuPDCS. On a benchmark dataset (CBLIB) comprising over 2,000 small-scale conic optimization instances, our method successfully solved the vast majority of problems, demonstrating better numerical stability compared with other methods. To assess scalability, we do experiments on three families of large-scale conic program problems—Fisher market equilibrium, Lasso regression, and multi-period portfolio optimization. The experiments demonstrate that cuPDCS scales more effectively to large-scale instances. Across scenarios involving varying cone counts, cuPDCS consistently produced high-quality solutions within reasonable computational time.

1.1 Related literature

The primal-dual hybrid gradient method (PDHG). The primal-dual hybrid gradient (PDHG) method was introduced in [19, 50] for solving general convex-concave saddle-point problems, of which the saddle-point formulation of conic programs is a special case. PDHG (with restarts) exhibits linear convergence on LPs, and its performance—including linear convergence rates and fast local convergence—has been extensively studied in [2, 32, 62, 42, 61, 59]. [43] introduces a Halpern restart scheme that achieves a complexity improvement of a constant order over the standard average-iteration restart scheme used in PDLP [1]. [63] establishes the convergence of restarted PDHG for general conic programs, showing that its performance is closely linked to the local geometry of sublevel sets near optimal solutions. [60] uses probabilistic analysis to establish a high-probability polynomial-time complexity result for the PDHG used on LPs. [41, 34] use PDHG to solve large-scale convex quadratic programs, which can also be equivalently reformulated as conic programs.

Other first-order methods for conic programs. Several other first-order methods have been developed for general conic programs. ABIP [38, 17] solves conic programs using an ADMM-based interior-point method applied to the homogeneous self-dual embedding of the conic program. SCS [49, 48] employs a similar ADMM-based approach to solve the homogeneous self-dual embedding. These ADMM-based methods require solving a linear system of similar form in each iteration, which

is typically handled either through matrix factorization or the conjugate gradient method. However, matrix factorizations suffer from scalability limitations and are not well-suited for parallel computing on GPUs. The conjugate gradient method, while avoiding explicit factorizations, requires multiple matrix-vector products per iteration, making the choice of tolerance for solving these linear systems a critical heuristic. We will present a comparison between PDCS and these methods in Section 5.

GPU acceleration for conic programs. The simplex method and interior-point methods generally do not benefit much from GPU acceleration due to their reliance on solving linear systems in each iteration [56, 25]. Recently, NVIDIA developed the first GPU-accelerated direct sparse solver (cuDSS) [16]. Based on cuDSS, very recently, [14] introduced CuClarabel, a GPU-accelerated interior-point method. The ADMM-based solver SCS [49, 48] also has a GPU implementation that leverages the conjugate gradient method for solving linear systems. However, these algorithms still face scalability issues for large-scale problems, as demonstrated in our comparison in Section 5.

During the final preparation of this manuscript, we became aware through personal conversations of a concurrent working project by Haihao Lu, Zedong Peng, and Jinwen Yang that proposes a GPU-implemented PDHG-based solver to solve large-scale second-order cone programs.

1.2 Outline

The paper is organized as follows. Section 1.3 introduces the notation used throughout the paper. Section 2 provides the conic program formulations considered in this paper and the PDHG iterations used as the base algorithm. Section 3 details the enhancement techniques incorporated into PDCS. Section 4 describes the customized computational schemes that leverage different levels of GPU architecture to efficiently handle various cone types. Finally, Section 5 presents numerical experiments comparing PDCS against other first-order methods and commercial solvers. All omitted proofs and additional details on numerical experiments are provided in the Appendix.

1.3 Notations

Throughout the paper, we use the following notations. Let $[n] := \{1, \dots, n\}$ for integer n . We use bold letters like \mathbf{v} to represent vectors and bold capital letters like \mathbf{A} to represent matrices. In general, we use subscripts to denote the coordinates of a vector without additional clarification. We define the l_q -norm for vector $\mathbf{v} \in \mathbb{R}^n$ as $\|\mathbf{v}\|_q = (\sum_{i=1}^n |\mathbf{v}_i|^q)^{1/q}$, where \mathbf{v}_i is the i -th entry of \mathbf{v} . For brevity, $\|\mathbf{v}\|$ stands for l_2 -norm. The inner product operator for two vectors is defined as $\langle \mathbf{u}, \mathbf{v} \rangle = \sum_{i=1}^n \mathbf{u}_i \mathbf{v}_i$. We denote the norm parameterized by matrix \mathbf{M} as $\|\mathbf{v}\|_{\mathbf{M}} = \sqrt{\mathbf{v}^\top \mathbf{M} \mathbf{v}}$. Denote the identity matrix as \mathbf{I} . Let $\mathbf{v}^+ = [(\mathbf{v}_1^+, \dots, \mathbf{v}_n^+)]$, where $\mathbf{v}_i^+ = \max\{\mathbf{v}_i, 0\}$ is the coordinate-wise positive part of a vector. Similar notation for the coordinate-wise negative part \mathbf{v}^- is defined by using $\mathbf{v}_i^- = \min\{\mathbf{v}_i, 0\}$. We denote the scaled cone as $\mathbf{D}\mathcal{K}$, which implies that $\mathbf{v} \in \mathbf{D}\mathcal{K}$ is equivalent to $\mathbf{D}^{-1}\mathbf{v} \in \mathcal{K}$. We use $\text{Proj}_{\mathcal{S}}(\mathbf{x}) = \text{argmin}_{\mathbf{y} \in \mathcal{S}} \|\mathbf{y} - \mathbf{x}\|$ to denote a projection operation that projects point \mathbf{x} to set \mathcal{S} . We use $\sigma_{\max}(\mathbf{A})$ to denote the largest singular values of \mathbf{A} .

Throughout this paper, we use the following notations for commonly used cones: $\mathbf{0}^d$ represents the zero cone, \mathcal{K}_+^d represents the non-negative cone, $\mathcal{K}_{\text{soc}}^{d+1}$ denotes the second-order cone, defined

as $\mathcal{K}_{\text{soc}}^{d+1} = \{(t, \mathbf{x}) \mid \mathbf{x} \in \mathbb{R}^d, t \in \mathbb{R}, \|\mathbf{x}\| \leq t\}$, $\mathcal{K}_{\text{rsoc}}^{d+2}$ denotes the rotated second-order cone, defined as $\mathcal{K}_{\text{rsoc}}^{d+2} = \{(x, y, \mathbf{z}) \mid x, y \in \mathbb{R}_+, \mathbf{z} \in \mathbb{R}^d, \|\mathbf{z}\|^2 \leq 2xy\}$, \mathcal{K}_{exp} denotes the exponential cone, defined as $\{(r, s, t) \in \mathbb{R}^3 \mid s > 0, t \geq s \cdot \exp(\frac{r}{s})\} \cup \{(r, s, t) \in \mathbb{R}^3 \mid s = 0, t \geq 0, r \leq 0\}$ and $\mathbb{S}_+^{d \times d}$ denotes the semi-definite cone, defined as $\mathbb{S}_+^{d \times d} = \{\mathbf{A} \in \mathbb{R}^{d \times d} : \mathbf{A} = \mathbf{A}^\top, \mathbf{x}^\top \mathbf{A} \mathbf{x} \geq 0, \forall \mathbf{x} \in \mathbb{R}^d \setminus \{\mathbf{0}\}\}$. The dual cone \mathcal{K}^* of \mathcal{K} is the set of non-negative dot products of $\mathbf{y} \in \mathbb{R}^d$ and $\mathbf{x} \in \mathcal{K}$, which is defined as $\mathcal{K}^* = \{\mathbf{y} \in \mathbb{R}^d : \langle \mathbf{y}, \mathbf{x} \rangle \geq 0, \forall \mathbf{x} \in \mathcal{K}\}$.

2 Preliminaries of Conic Optimization and PDHG

In this section, we present the formulation of the conic optimization problems (conic programs) considered in this paper, along with their corresponding dual problems and equivalent saddle-point formulations. In Section 2.1, we outline the iterations of the basic Primal-Dual Hybrid Gradient (PDHG) method for these conic programs.

We consider the following conic program:

$$\min_{\substack{\mathbf{x}=(\mathbf{x}_1, \mathbf{x}_2): \\ \mathbf{x}_1 \in \mathbb{R}^{n_1}, \mathbf{x}_2 \in \mathbb{R}^{n_2}}} \langle \mathbf{c}, \mathbf{x} \rangle \quad \text{s. t.} \quad \mathbf{G}\mathbf{x} - \mathbf{h} \in \mathcal{K}_d^*, \mathbf{l} \leq \mathbf{x}_1 \leq \mathbf{u}, \mathbf{x}_2 \in \mathcal{K}_p, \quad (\text{P})$$

where $\mathbf{G} \in \mathbb{R}^{m \times n}$ is the constraint matrix, $\mathbf{l} \in (\mathbb{R} \cup \{-\infty\})^{n_1}$, $\mathbf{u} \in (\mathbb{R} \cup \{\infty\})^{n_2}$ denote the lower bound and upper bound for the decision variable components \mathbf{x}_1 and \mathbf{x}_2 . The set \mathcal{K}_p denotes the primal cone, which is a Cartesian product of nonempty closed smaller cones: $\mathcal{K}_1 \times \mathcal{K}_2 \times \dots \times \mathcal{K}_{l_p}$, where l_p denotes the number of the smaller cones. These smaller cones include the zero cone $\mathbf{0}^d$, the nonnegative orthant \mathbb{R}_+^d , the second-order cone $\mathbb{R}_{\text{soc}}^{d+1}$, the exponential cone \mathcal{K}_{exp} , the rotated second-order cone $\mathcal{K}_{\text{rsoc}}^{d+2}$ and the dual exponential cone $\mathcal{K}_{\text{exp}}^*$, and we call them *disciplined cones*. Our algorithm also applies to the semidefinite cone ($\mathbb{S}_+^{d \times d}$). As for \mathcal{K}_d^* , it denotes the dual cone of \mathcal{K}_d , because the dual problem can be written as a problem of \mathcal{K}_d expressed as follows:

$$\begin{aligned} \max_{\substack{\mathbf{y}, \boldsymbol{\lambda}=(\boldsymbol{\lambda}_1, \boldsymbol{\lambda}_2): \\ \mathbf{y} \in \mathbb{R}^m, \boldsymbol{\lambda}_1 \in \mathbb{R}^{n_1}, \boldsymbol{\lambda}_2 \in \mathbb{R}^{n_2}}} & \langle \mathbf{y}, \mathbf{h} \rangle + \mathbf{l}^\top \boldsymbol{\lambda}_1^+ + \mathbf{u}^\top \boldsymbol{\lambda}_1^- , \\ \text{s. t.} & \quad \mathbf{c} - \mathbf{G}^\top \mathbf{y} = \boldsymbol{\lambda}, \mathbf{y} \in \mathcal{K}_d, \boldsymbol{\lambda}_1 \in \Lambda, \boldsymbol{\lambda}_2 \in \mathcal{K}_p^*, \end{aligned} \quad (\text{D})$$

where

$$\Lambda := \Lambda_1 \times \Lambda_2 \times \dots \times \Lambda_{n_1} \quad \text{and} \quad \Lambda_i := \begin{cases} \{0\}, & \text{if } \mathbf{l}_i = -\infty, \mathbf{u}_i = +\infty \\ \mathbb{R}^-, & \text{if } \mathbf{l}_i = -\infty, \mathbf{u}_i \in \mathbb{R} \\ \mathbb{R}^+, & \text{if } \mathbf{l}_i \in \mathbb{R}, \mathbf{u}_i = +\infty \\ \mathbb{R}, & \text{if otherwise} \end{cases} \quad \text{for } i = 1, 2, \dots, n_1. \quad (1)$$

Similarly, the \mathcal{K}_d can be expressed as a Cartesian product of smaller disciplined cones: $\mathcal{K}_d := \mathcal{K}_1 \times \mathcal{K}_2 \times \dots \times \mathcal{K}_{l_d}$. And its dual cone \mathcal{K}_d^* is correspondingly given by $\mathcal{K}_1^* \times \mathcal{K}_2^* \times \dots \times \mathcal{K}_{l_d}^*$.

The problem (P) has an equivalent primal-dual formulation, expressed as the following saddle-

point problem on the Lagrangian $\mathcal{L}(\mathbf{x}, \mathbf{y})$:

$$\min_{\mathbf{x} \in \mathcal{X}} \max_{\mathbf{y} \in \mathcal{Y}} \mathcal{L}(\mathbf{x}, \mathbf{y}) := \langle \mathbf{c}, \mathbf{x} \rangle - \langle \mathbf{y}, \mathbf{G}\mathbf{x} - \mathbf{h} \rangle, \quad (\text{PD})$$

where $\mathcal{X} := [\mathbf{l}, \mathbf{u}] \times \mathcal{K}_p$ and $\mathcal{Y} := \mathcal{K}_d$. A saddle point (\mathbf{x}, \mathbf{y}) of (PD) corresponds to an optimal primal solution \mathbf{x} for (P) and an optimal dual solution $(\mathbf{y}, \mathbf{c} - \mathbf{G}^\top \mathbf{y})$ for (D).

According to the Karush-Kuhn-Tucker conditions, for any $(\mathbf{x}, \mathbf{y}, \boldsymbol{\lambda})$ satisfying $\mathbf{c} - \mathbf{G}^\top \mathbf{y} = \boldsymbol{\lambda}$, we define the following optimality error metrics:

$$\begin{aligned} \text{err}_{\text{abs},p}(\mathbf{x}) &:= \left\| (\mathbf{G}\mathbf{x} - \mathbf{h}) - \text{Proj}_{\mathcal{K}_d^*} \{ \mathbf{G}\mathbf{x} - \mathbf{h} \} \right\|, \\ \text{err}_{\text{abs},d}(\boldsymbol{\lambda}_1, \boldsymbol{\lambda}_2) &:= \sqrt{\| \boldsymbol{\lambda}_1 - \text{Proj}_{\Lambda} \{ \boldsymbol{\lambda}_1 \} \|^2 + \| \boldsymbol{\lambda}_2 - \text{Proj}_{\mathcal{K}_p^*} \{ \boldsymbol{\lambda}_2 \} \|^2}, \\ \text{err}_{\text{abs},\text{gap}}(\mathbf{x}, \boldsymbol{\lambda}_1, \boldsymbol{\lambda}_2) &:= \left| \langle \mathbf{c}, \mathbf{x} \rangle - \left(\mathbf{y}^\top \mathbf{h} + \mathbf{l}^\top \boldsymbol{\lambda}_1^+ + \mathbf{u}^\top \boldsymbol{\lambda}_1^- \right) \right|. \end{aligned} \quad (2)$$

It is important to note that the above definitions only involve \mathbf{x} and $\boldsymbol{\lambda}$ for simplicity because \mathbf{y} and $\boldsymbol{\lambda}$ correspond to each other one-on-one when $\mathbf{c} - \mathbf{G}^\top \mathbf{y} = \boldsymbol{\lambda}$. These three metrics in (2) quantify the primal infeasibility $\text{err}_{\text{abs},p}(\mathbf{x})$, dual infeasibility $\text{err}_{\text{abs},d}(\boldsymbol{\lambda}_1, \boldsymbol{\lambda}_2)$, and primal-dual gap $\text{err}_{\text{abs},\text{gap}}(\mathbf{x}, \boldsymbol{\lambda}_1, \boldsymbol{\lambda}_2)$ in terms of the ℓ_2 -norm. Alternative metrics using other norms may also be employed in subsequent sections.

2.1 PDHG for conic programs

PDCS uses PDHG as its base algorithm and one iteration of PDHG for solving (PD) at iterate $\mathbf{z} = (\mathbf{x}, \mathbf{y})$ (denoted by $\text{OnePDHG}(\mathbf{z})$) is given by:

$$\hat{\mathbf{z}} = \text{OnePDHG}(\mathbf{z}) := \begin{cases} \hat{\mathbf{x}} = \text{Proj}_{[\mathbf{l}, \mathbf{u}] \times \mathcal{K}_p} \{ \mathbf{x} - \tau(\mathbf{c} - \mathbf{G}^\top \mathbf{y}) \} \\ \hat{\mathbf{y}} = \text{Proj}_{\mathcal{K}_d} \{ \mathbf{y} + \sigma(\mathbf{h} - \mathbf{G}(2\hat{\mathbf{x}} - \mathbf{x})) \} \end{cases}, \quad (3)$$

where τ and σ are the primal and dual step sizes, respectively. It has been proven by [10, 39, 63] et al. that the iterates generated by (3) globally converge to the saddle point of (PD) and achieve a linear convergence rate for LP problems.

The one PDHG iteration (3) does not require any matrix factorization and the core operations consist only of the matrix-vector multiplications and two projections onto $[\mathbf{l}, \mathbf{u}] \times \mathcal{K}_p$ and \mathcal{K}_d . The matrix-vector multiplication is cheaper than matrix factorization in both memory usage and computational complexity. Moreover, projections onto the Cartesian product of disciplined cones can be performed in parallel. Specifically, each component of the vector (corresponding to different disciplined cones) can be projected independently, i.e.,

$$\text{Proj}_{\mathcal{K}_1 \times \dots \times \mathcal{K}_l}(\mathbf{x}) = [\text{Proj}_{\mathcal{K}_1}(\mathbf{x}_{[1]})^\top, \dots, \text{Proj}_{\mathcal{K}_l}(\mathbf{x}_{[l]})^\top]^\top, \quad (4)$$

where $\mathbf{x}_{[i]}$ denotes the component of \mathbf{x} corresponding to the i -th disciplined cone \mathcal{K}_i . Table 1

summarizes the projection operations for the disciplined cones considered, as well as for the positive semidefinite cone. It can be observed from Table 1 that the projections onto $\mathbf{0}^d$ and \mathbb{R}_+^d are trivial.

Table 1: Euclidean projections onto different disciplined cones

Disciplined Cone	Projection Operation
Zero Cone ($\mathbf{0}^d$)	$\text{Proj}_{\{\mathbf{0}^d\}}\{\mathbf{x}\} = \mathbf{0}$
Nonnegative Cone (\mathbb{R}_+^d)	$\text{Proj}_{\mathbb{R}_+^d}\{\mathbf{x}\} = \mathbf{x}^+$
Second-order Cone ($\mathcal{K}_{\text{soc}}^{d+1}$)	$\text{Proj}_{\mathcal{K}_{\text{soc}}^{d+1}}(t, \mathbf{x}) = \begin{cases} 0, & \ \mathbf{x}\ \leq -t, \\ (t, \mathbf{x}), & \ \mathbf{x}\ \leq t, \\ \frac{1+t/\ \mathbf{x}\ }{2}(\ \mathbf{x}\ , \mathbf{x}), & \ \mathbf{x}\ \geq t . \end{cases}$
Exponential Cone (\mathcal{K}_{exp})	A root finding problem [22]
Positive Semidefinite Cone ($\mathbb{S}_+^{d \times d}$)	$\text{Proj}_{\mathbb{S}_+^{d \times d}}(\mathbf{X}) = \mathbf{U}\mathbf{\Lambda}^+\mathbf{U}^\top$ for $\mathbf{X} = \mathbf{U}\mathbf{\Lambda}\mathbf{U}^\top$ and $\mathbf{U}\mathbf{U}^\top = \mathbf{I}$

As for the second-order cone $\mathcal{K}_{\text{soc}}^{d+1}$, the most time-consuming computations can be reduced to a Euclidean norm computation (i.e., a vector-vector product). For the exponential cone \mathcal{K}_{exp} , the cost of projection onto this cone is almost constant because of its low dimensionality. The only expensive projection above is the projection onto the $\mathbb{S}_+^{d \times d}$, which requires a singular value decomposition. This can be computationally prohibitive for large d . In addition to the five cone projections presented in Table 1, the rotated second-order cone ($\mathcal{K}_{\text{rsoc}}^{d+2}$) and the dual exponential cone ($\mathcal{K}_{\text{exp}}^*$) can be projected onto pretty efficiently. Notably, the $\mathcal{K}_{\text{rsoc}}^{d+2}$ is equivalent to the second-order cone via reformulation, and the projection onto the $\mathcal{K}_{\text{exp}}^*$ closely resembles that of the exponential cone. As a result, for most typical conic programs except the ones involving semi-definite cones, PDHG remains a fully matrix-free method, making it scalable for most large-scale conic program problems.

3 A Practical Primal-Dual Conic Programming Solver

In this section, we present the algorithmic enhancements used in PDCS. Built upon the basic PDHG framework, PDCS integrates several techniques, including adaptive step-size selection (Section 3.1), adaptive reflected Halpern iteration (Section 3.2), adaptive restart (Section 3.3), and primal weight updates (Section 3.4). The overall algorithmic framework is summarized in Algorithm 1, with each enhancement described in detail in the following subsections. In addition, PDCS also applies diagonal preconditioning to improve the conditioning of problem instances. This preconditioning procedure is described in Section 3.5.

To briefly summarize the main components in Algorithm 1: the function **AdaptiveStepPDHG** in Line 4 performs a line search to determine an appropriate step size; the function **AdaptiveReflection** in Line 5 computes the reflection coefficient; Lines 6 and 7 perform a reflected Halpern iteration and weighted averaging of iterates; and the function **GetRestartCandidate** in Line 8 selects a candidate for restarting based on either the normalized duality gap or KKT error. At each outer iteration, the primal weight ω is updated based on the progress of primal and dual iterates, and this weight plays a central role in balancing the primal and dual step sizes via the function **AdaptiveStepPDHG**.

Algorithm 1 Primal Dual Conic Programming Solver (PDCS) (without preconditioning)

Require: $\mathbf{z}^{0,0} = (\mathbf{x}^{0,0}, \mathbf{y}^{0,0})$, total iteration $\bar{k} \leftarrow 0$, step-size $\hat{\eta}^{0,0} \leftarrow 1/\|\mathbf{G}\|_\infty$, primal weight $\omega^0 \leftarrow \text{InitializePrimalWeight}(\mathbf{c}, \mathbf{h})$ (Section 3.4).

```

1: while Termination criteria do not hold do
2:    $k \leftarrow 0$ 
3:   while both Restart condition (Section 3.3) and the termination criteria do not hold do
4:      $\hat{\mathbf{z}}^{t,k+1}, \eta^{t,k+1}, \hat{\eta}^{t,k+1}, \bar{k} \leftarrow \text{AdaptiveStepPDHG}(\mathbf{z}^{t,k}, \omega^t, \hat{\eta}^{t,k}, \bar{k})$   $\triangleright$  Section 3.1
5:      $\beta^{t,k} \leftarrow \text{AdaptiveReflection}(\hat{\mathbf{z}}^{t,k+1})$   $\triangleright$  Section 3.2
6:      $\mathbf{z}^{t,k+1} = \frac{k+1}{k+2}((1 + \beta^{t,k})\hat{\mathbf{z}}^{t,k} - \beta^{t,k}\mathbf{z}^{t,k}) + \frac{1}{k+2}\mathbf{z}^{t,0}$ 
7:      $\bar{\mathbf{z}}^{t,k+1} \leftarrow \frac{1}{\sum_{i=1}^{k+1} \eta^{t,i}} \sum_{i=1}^{k+1} \eta^{t,i} \mathbf{z}^{t,i}$ 
8:      $\mathbf{z}_c^{t,k+1} \leftarrow \text{GetRestartCandidate}(\mathbf{z}^{t,k+1}, \bar{\mathbf{z}}^{t,k+1})$   $\triangleright$  Section 3.3
9:      $k \leftarrow k + 1$ 
10:    Restart  $\mathbf{z}^{t+1,0} \leftarrow \mathbf{z}_c^{t,k}, t \leftarrow t + 1$ 
11:     $\omega^t \leftarrow \text{PrimalWeightUpdate}(\mathbf{z}^{t,0}, \mathbf{z}^{t-1,0}, \omega^{t-1})$   $\triangleright$  Section 3.4

```

3.1 Adaptive step-size

To ensure global convergence in theory, the step-sizes τ and σ must satisfy the condition $\tau\sigma \leq \frac{1}{\|\mathbf{G}\|}$ [10]. However, this requirement is often overly conservative in practice. To improve empirical performance, PDCS employs a line search heuristic similar to the one used in PDLP [1], allowing it to adaptively choose step-sizes. Specifically, PDCS selects the parameters as follows:

$$\tau = \frac{\eta}{\omega}, \quad \sigma = \eta\omega, \quad \eta \leq \frac{\|\mathbf{z}^{t+1} - \mathbf{z}^t\|_\omega^2}{2|(\mathbf{y}^{t+1} - \mathbf{y}^t)^\top \mathbf{G}(\mathbf{x}^{t+1} - \mathbf{x}^t)|}, \quad (5)$$

where $\|\mathbf{z}\|_\omega := \sqrt{\omega \|\mathbf{x}\|^2 + \frac{\|\mathbf{y}\|^2}{\omega}}$, and ω is the primal weight.

The update of η is carried out by the procedure described in Function 2. Here, \bar{k} records the total number of PDHG iterations and controls how aggressively η is adjusted. Compared to PDLP, which uses the inner-loop count k to control the adjustment rate, PDCS uses \bar{k} , resulting in more conservative updates in early iterations [1].

Function 2 AdaptiveStepPDHG($(\mathbf{x}, \mathbf{y}), \omega, \eta, \bar{k}$)

```

1: while True do
2:    $\hat{\mathbf{x}} = \text{Proj}_{[\mathbf{l}, \mathbf{u}] \times \mathcal{K}_p} \left\{ \mathbf{x} - \frac{\eta}{\omega}(\mathbf{c} - \mathbf{G}^\top \mathbf{y}) \right\}$ 
3:    $\hat{\mathbf{y}} = \text{Proj}_{\mathcal{K}_d} \left\{ \mathbf{y} + \eta\omega(\mathbf{h} - \mathbf{G}(2\hat{\mathbf{x}} - \mathbf{x})) \right\}$ 
4:    $\bar{\eta} \leftarrow \frac{1}{2} \frac{\|(\hat{\mathbf{x}} - \mathbf{x}, \hat{\mathbf{y}} - \mathbf{y})\|_\omega^2}{|(\hat{\mathbf{y}} - \mathbf{y})^\top \mathbf{G}(\hat{\mathbf{x}} - \mathbf{x})|}$ 
5:    $\eta' \leftarrow \min \left\{ (1 - (\bar{k} + 1)^{-0.3})\bar{\eta}, (1 + (\bar{k} + 1)^{-0.6})\eta \right\}$ 
6:   if  $\eta < \bar{\eta}$  then
7:     return  $(\hat{\mathbf{x}}, \hat{\mathbf{y}}), \eta, \eta', \bar{k}$ 
8:    $\eta \leftarrow \eta', \bar{k} \leftarrow \bar{k} + 1$ 

```

3.2 Adaptive reflected Halpern iteration

Line 6 in Algorithm 1 implements a reflected Halpern iteration. A similar technique has been used in practical first-order LP solvers such as HPR-LP [12] and r²HPDHG [43], where it has demonstrated significant empirical acceleration. The standard Halpern iteration involves averaging the current iterate (typically $\hat{\mathbf{z}}^{t,k}$) with the initial point $\mathbf{z}^{t,0}$ of the current inner loop. This anchoring mechanism mitigates oscillations in PDHG iterates and has been shown to yield improved worst-case convergence rates. In this setting, the point $\mathbf{z}^{t,0}$ serves as a fixed anchor. Originally introduced by [28], Halpern iteration has recently been recognized again for its role in accelerating a range of minimax optimization and fixed-point methods; see, e.g., [65].

The idea behind the reflected Halpern iteration is to apply this anchoring technique not directly to $\hat{\mathbf{z}}^{t,k}$, but to an extrapolated point between the newly computed iterate $\hat{\mathbf{z}}^{t,k}$ and the previous iterate $\mathbf{z}^{t,k}$. Specifically, Line 6 replaces $\hat{\mathbf{z}}^{t,k}$ with $(1 + \beta^{t,k})\hat{\mathbf{z}}^{t,k} - \beta^{t,k}\mathbf{z}^{t,k}$, where β is the reflection parameter. It has been theoretically shown that the reflected Halpern iteration can further accelerate convergence in general fixed-point methods, including PDHG, see [54, 37, 43].

In practice, larger values of β correspond to more aggressive extrapolation, which can accelerate convergence but may also introduce instability and oscillations if set too high. To balance acceleration with stability, PDCS adaptively adjusts the reflection coefficient based on the observed progress of iterates. When the KKT error is large, indicating that the iterate is still far from optimality, a smaller coefficient is selected to promote conservative and stable updates. As the iterates begin to converge and the KKT error decreases, a larger coefficient is used to speed up progress. For conic programs, PDCS uses the following rule to select the reflection parameter based on the KKT error at $\hat{\mathbf{z}}^{t,k} = (\hat{\mathbf{x}}^{t,k}, \hat{\mathbf{y}}^{t,k})$:

$$\text{AdaptiveReflection}(\hat{\mathbf{z}}^{t,k}) = \text{Proj}_{[0,1]} \left(-0.1 \cdot \log_{10} \left(\max\text{Err}(\hat{\mathbf{z}}^{t,k}) \right) + 0.2 \right), \quad (6)$$

where $\max\text{Err}(\cdot)$ measures the overall optimality error and is defined by

$$\max\text{Err}(\mathbf{z}) := \max\{\text{err}_{\text{rel,p}}(\mathbf{x}), \text{err}_{\text{rel,d}}(\boldsymbol{\lambda}_1, \boldsymbol{\lambda}_2), \text{err}_{\text{rel,gap}}(\mathbf{x}, \boldsymbol{\lambda}_1, \boldsymbol{\lambda}_2)\}. \quad (7)$$

Here $\text{err}_{\text{rel,p}}(\mathbf{x})$, $\text{err}_{\text{rel,d}}(\boldsymbol{\lambda}_1, \boldsymbol{\lambda}_2)$, $\text{err}_{\text{rel,gap}}(\mathbf{x}, \boldsymbol{\lambda}_1, \boldsymbol{\lambda}_2)$ are relative primal infeasibility, relative dual infeasibility and relative primal-dual gap:

$$\begin{aligned} \text{err}_{\text{rel,p}}(\mathbf{x}) &:= \frac{\text{err}_{\text{abs,p}}(\mathbf{x})}{1 + \|\mathbf{h}\|_1}, \quad \text{err}_{\text{rel,d}}(\boldsymbol{\lambda}_1, \boldsymbol{\lambda}_2) := \frac{\text{err}_{\text{abs,d}}(\boldsymbol{\lambda}_1, \boldsymbol{\lambda}_2)}{1 + \|\mathbf{c}\|_1}, \\ \text{err}_{\text{rel,gap}}(\mathbf{x}, \boldsymbol{\lambda}_1, \boldsymbol{\lambda}_2) &:= \frac{\text{err}_{\text{abs,gap}}(\mathbf{x}, \boldsymbol{\lambda}_1, \boldsymbol{\lambda}_2)}{1 + |\langle \mathbf{c}, \mathbf{x} \rangle| + |\mathbf{y}^\top \mathbf{h} + \mathbf{I}^\top \boldsymbol{\lambda}_1^\top + \mathbf{u}^\top \boldsymbol{\lambda}_1|}. \end{aligned} \quad (8)$$

The absolute errors in the numerators are defined in (2). We adopt these relative errors because they are invariant under scalar rescaling of problem data and demonstrate more stable empirical performance in our experiments.

3.3 Adaptive restart

The restart technique resets the anchor point used in the Halpern iteration to a carefully selected point and simultaneously updates the primal weight ω^t (see Section 3.4). It has been proven that PDHG with restarts (either average-iterate restarts or Halpern restarts) achieves linear convergence for LP problems [2, 43]. For general conic programs, [63] establishes global convergence of PDHG with average-iterate restarts, and similar results may be extended to Halpern-iteration restarts using the techniques in [43]. Empirical studies have also shown that restart strategies can significantly improve the practical performance of PDHG [1, 2].

To select the new anchor point, PDCS evaluates the normalized duality gap, which serves as a surrogate for optimality. This metric is defined as follows:

Definition 1 (normalized duality gap [63]). For any $\mathbf{z} = (\mathbf{x}, \mathbf{y}) \in \mathcal{X} \times \mathcal{Y}$, $r > 0$, and step-sizes $\tau > 0$, $\sigma > 0$ satisfying $\tau\sigma \leq (\sigma_{\max}(\mathbf{G}))^{-2}$, define $\mathbf{M} := \begin{pmatrix} \frac{1}{\tau}\mathbf{I} & -\mathbf{G}^\top \\ -\mathbf{G} & \frac{1}{\sigma}\mathbf{I} \end{pmatrix}$ and $\mathcal{B}(r; \mathbf{z}) := \{\hat{\mathbf{z}} := (\hat{\mathbf{x}}, \hat{\mathbf{y}}) : \hat{\mathbf{x}} \in \mathcal{X}, \hat{\mathbf{y}} \in \mathcal{Y}, \|\mathbf{z} - \hat{\mathbf{z}}\|_{\mathbf{M}} \leq r\}$, then the normalized duality gap is given by $\rho(r; \mathbf{z}) := \frac{1}{r} \sup_{\hat{\mathbf{z}} \in \mathcal{B}(r; \mathbf{z})} [\mathcal{L}(\mathbf{x}, \hat{\mathbf{y}}) - \mathcal{L}(\hat{\mathbf{x}}, \mathbf{y})]$.

The τ and σ above correspond to the current step sizes $\tau^{t,k}$ and $\sigma^{t,k}$. [2, 63] show that the above normalized duality gap $\rho(r; \mathbf{z})$ serves as a measurement of the optimality of solution \mathbf{z} . However, computing $\rho(r; \mathbf{z})$ exactly involves a nontrivial projection onto $\mathcal{X} \times \mathcal{Y}$ under the \mathbf{M} -norm, which is computationally expensive. To alleviate this, we approximate the duality gap by replacing \mathbf{M} with a diagonal surrogate matrix $\mathbf{N} := \begin{pmatrix} \frac{1}{\tau}\mathbf{I} & \\ & \frac{1}{\sigma}\mathbf{I} \end{pmatrix}$ and denote the resulting approximate gap as $\rho^{\mathbf{N}}(\cdot, \cdot)$. This approximation $\rho^{\mathbf{N}}(\cdot, \cdot)$ is equivalent to $\rho(\cdot, \cdot)$ under a constant factor and can be efficiently computed using a bisection search method [2, 63]. The details of the computation method are deferred to Appendix A.

In PDCS, we compare the approximate normalized duality gaps of $\mathbf{z}^{t,k+1}$ and $\bar{\mathbf{z}}^{t,k+1}$, and select the one with the smaller gap as the new anchor point:

$$\begin{aligned} & \text{GetRestartCandidate}(\mathbf{z}^{t,k+1}, \bar{\mathbf{z}}^{t,k+1}) \\ &= \begin{cases} \mathbf{z}^{t,k+1} & \rho^{\mathbf{N}}(\|\mathbf{z}^{t,k+1} - \mathbf{z}^{t,0}\|_{\mathbf{N}}; \mathbf{z}^{t,k+1}) \leq \rho^{\mathbf{N}}(\|\bar{\mathbf{z}}^{t,k+1} - \mathbf{z}^{t,0}\|_{\mathbf{N}}; \bar{\mathbf{z}}^{t,k+1}) \\ \bar{\mathbf{z}}^{t,k+1} & \text{otherwise} \end{cases} \end{aligned}$$

Let $\mathbf{z}_c^{t,k+1}$ denote the resulting restart candidate. A restart to $\mathbf{z}_c^{t,k+1}$ is triggered whenever its approximate normalized duality gap satisfies any of the following conditions. Let $\beta_{\text{sufficient}} = 0.4$, $\beta_{\text{necessary}} = 0.8$, and $\beta_{\text{artificial}} = 0.223$, and define the **Restart Condition** to hold if one of the following is true:

1. (Sufficient decay) $\rho^{\mathbf{N}}(\|\mathbf{z}_c^{t,k+1} - \mathbf{z}^{t,0}\|_{\mathbf{N}}; \mathbf{z}_c^{t,k+1}) \leq \beta_{\text{sufficient}} \cdot \rho^{\mathbf{N}}(\|\mathbf{z}^{t,0} - \mathbf{z}^{t-1,0}\|_{\mathbf{N}}; \mathbf{z}^{t,0})$
2. (Necessary decay + no local progress) $\rho^{\mathbf{N}}(\|\mathbf{z}_c^{t,k+1} - \mathbf{z}^{t,0}\|_{\mathbf{N}}; \mathbf{z}_c^{t,k+1}) > \rho^{\mathbf{N}}(\|\mathbf{z}_c^{t,k} - \mathbf{z}^{t,0}\|_{\mathbf{N}}; \mathbf{z}_c^{t,k})$

$$\text{and } \rho^{\mathbf{N}} \left(\left\| \mathbf{z}_c^{t,k+1} - \mathbf{z}^{t,0} \right\|_{\mathbf{N}} ; \mathbf{z}_c^{t,k+1} \right) \leq \beta_{\text{necessary}} \cdot \rho^{\mathbf{N}} \left(\left\| \mathbf{z}^{t,0} - \mathbf{z}^{t-1,0} \right\|_{\mathbf{N}} ; \mathbf{z}^{t,0} \right)$$

3. (Long inner loop) $k \geq \beta_{\text{artificial}} \cdot \bar{k}$.

A similar adaptive restart approach has also been used in first-order LP solvers PDLP [1], cuPDLP [40] and cuPDLP-c [44].

However, for general conic programs, numerical issues are more severe, particularly when evaluating $\rho^{\mathbf{N}}$ for cones beyond LP cones. In some cases, especially when the actual gap value is very small, the bisection method may produce negative outputs due to floating-point inaccuracies. When this occurs, PDCS switches to an alternative criterion based on the weighted KKT error.

$$\text{KKT}_{\omega}(\mathbf{z}) = \sqrt{\omega^2 \text{err}_{\text{abs,p}}(\mathbf{x})^2 + \frac{1}{\omega^2} \text{err}_{\text{abs,d}}(\boldsymbol{\lambda}_1, \boldsymbol{\lambda}_2)^2 + \text{err}_{\text{abs,gap}}(\mathbf{x}, \boldsymbol{\lambda}_1, \boldsymbol{\lambda}_2)^2}, \quad (9)$$

where $\text{err}_{\text{abs,p}}$, $\text{err}_{\text{abs,d}}$, $\text{err}_{\text{abs,gap}}$ are as defined in (7), and the dual variables $\boldsymbol{\lambda}_1, \boldsymbol{\lambda}_2$ are recovered from \mathbf{y} using the linear relation in (D). When numerical issues happen, all instances of $\rho^{\mathbf{N}}(r; \mathbf{z})$ in both `GetRestartCandidate` and `RestartCondition` are replaced with $\text{KKT}_{\omega}(\mathbf{z})$.

3.4 Primal weight adjustment

As shown in Function 2, the primal weight is used to balance the primal and dual step-sizes. A larger primal weight leads to a smaller primal step-size τ and a larger dual step-size σ . The update strategy follows a similar approach to that used in PDLP [1], relying on the relative changes in the primal and dual variables. In PDCS, the primal weight is updated only at the beginning of each new restart. The primal weight is initialized using: $\text{InitializePrimalWeight}(\mathbf{c}, \mathbf{h}) := \begin{cases} \frac{\|\mathbf{c}\|_2}{\|\mathbf{h}\|_2}, & \|\mathbf{c}\|_2, \|\mathbf{h}\|_2 > 10^{-10} \\ 1 & \text{otherwise} \end{cases}$.

The update at the beginning of a new restart is defined as:

$$\text{PrimalWeightUpdate}(\mathbf{z}^{t,0}, \mathbf{z}^{t-1,0}, \omega^{t-1}) := \begin{cases} \exp \left(\theta \log \left(\frac{\Delta_y^t}{\Delta_x^t} \right) + (1 - \theta) \log (\omega^{t-1}) \right) & \Delta_x^t, \Delta_y^t > 10^{-10} \\ \omega^{t-1} & \text{otherwise} \end{cases},$$

where $\Delta_x^t = \|\mathbf{x}^{t,0} - \mathbf{x}^{t-1,0}\|$ and $\Delta_y^t = \|\mathbf{y}^{t,0} - \mathbf{y}^{t-1,0}\|$ denote the changes in the primal and dual variables, respectively. In practice, we set $\theta = 0.5$. Occasionally, we observe that the solver can become unstable when the primal weight grows too large or too small, causing imbalanced updates between the primal and dual iterates. To mitigate this, if $\omega > 10^5$ or $\omega < 10^{-5}$, we reset ω to its initial value computed by `InitializePrimalWeight`.

3.5 Diagonal rescaling and projections onto rescaled cones

Like many other first-order methods, the practical performance of PDCS is closely tied to the conditioning of the problem instance. One common strategy is diagonal rescaling, which may improve the condition number of the problem while preserving the sparsity pattern. This technique

has become a standard step in many first-order solvers for LPs, including PDLP [1], cuPDLP [40], and ABIP [17].

We rescale the constraint matrix $\mathbf{G} \in \mathbb{R}^{m \times n}$ to $\hat{\mathbf{G}} = \mathbf{D}_1 \mathbf{G} \mathbf{D}_2$, where \mathbf{D}_1 and \mathbf{D}_2 are positive diagonal matrices. The corresponding rescaled optimization problem is:

$$\min \quad \langle \hat{\mathbf{c}}, \tilde{\mathbf{x}} \rangle, \quad \text{s.t.} \quad \hat{\mathbf{G}}\tilde{\mathbf{x}} - \hat{\mathbf{h}} \in \hat{\mathcal{K}}_d^*, \quad \hat{\mathbf{l}} \leq (\tilde{\mathbf{x}})_{[n_1]} \leq \hat{\mathbf{u}}, \quad (\tilde{\mathbf{x}})_{[n] \setminus [n_1]} \in \hat{\mathcal{K}}_p \quad (10)$$

where the transformed data and cones are defined as: $\hat{\mathbf{c}} := \mathbf{c} \mathbf{D}_2$, $\hat{\mathbf{G}} := \mathbf{D}_1 \mathbf{G} \mathbf{D}_2$, $\hat{\mathbf{h}} := \mathbf{D}_1 \mathbf{h}$, $\hat{\mathbf{l}} := \mathbf{D}_2^{-1} \mathbf{l}$, $\hat{\mathbf{u}} := \mathbf{D}_2^{-1} \mathbf{u}$, $\hat{\mathcal{K}}_d^* := \mathbf{D}_1 \mathcal{K}_d^*$ and $\hat{\mathcal{K}}_p := \mathbf{D}_2^{-1} \mathcal{K}_p$. For any optimal solution $\tilde{\mathbf{x}}$ of the rescaled problem (10), an optimal solution of the original problem (P) can be recovered as $\mathbf{x} = \mathbf{D}_2 \tilde{\mathbf{x}}$. Following the practice of PDLP, we perform several initial iterations of Ruiz rescaling [52], followed by one iteration of Pock-Chambolle rescaling [10].

The full PDCS framework with diagonal rescaling is summarized in Algorithm 3.

Algorithm 3 Primal Dual Conic Solver (PDCS) (with preconditioning)

- 1: Compute rescaled instance data $\hat{\mathbf{c}}, \hat{\mathbf{G}}, \hat{\mathbf{h}}, \hat{\mathbf{l}}$ and $\hat{\mathbf{u}}$.
 - 2: Use Algorithm 1 to solve the rescaled problem (10) and get solution $\tilde{\mathbf{x}}$ and $\tilde{\mathbf{y}}$.
 - 3: Output solution for (P): $\mathbf{x} = \mathbf{D}_2 \tilde{\mathbf{x}}$ and $\mathbf{y} = \mathbf{D}_1 \tilde{\mathbf{y}}$.
-

This rescaling reformulates the problem in terms of non-standard cones $\hat{\mathcal{K}}_p$ and $\hat{\mathcal{K}}_d^*$. For LPs, the rescaled nonnegative cones remain nonnegative cones, so projections remain straightforward. However, in general conic programs, diagonal rescaling introduces new challenges. Specifically, after rescaling, projections onto second-order cones no longer admit closed-form solutions, and projections onto exponential cones require more intricate calculations.

Projection onto rescaled second-order cones. After introducing the diagonal rescaling $\mathbf{D} = \begin{pmatrix} \mathbf{d}_1 & & \\ & \ddots & \\ & & \mathbf{d}_{n+1} \end{pmatrix}$, the projection onto the second-order cone is equivalent to solving the following optimization problem:

$$\text{Proj}_{\mathbf{D}\mathcal{K}_{\text{soc}}} \{(t, \mathbf{x})\} = \underset{(s, \mathbf{y}) \in \mathbb{R}^{n+1}}{\text{argmin}} \quad \frac{1}{2} \|(t, \mathbf{x}) - (s, \mathbf{y})\|^2, \quad \text{s.t.} \quad \|\hat{\mathbf{D}}^{-1} \mathbf{y}\|^2 \leq s^2, \quad s \geq 0, \quad (11)$$

where $(t, \mathbf{x}) \in \mathbb{R}^{n+1}$, and $\hat{\mathbf{D}} = \begin{pmatrix} \hat{\mathbf{d}}_2 & & \\ & \ddots & \\ & & \hat{\mathbf{d}}_{n+1} \end{pmatrix}$ with $\hat{\mathbf{d}}_i = \mathbf{d}_i / \mathbf{d}_1$, and \mathbf{d}_i denotes the i -th entry in the diagonal of \mathbf{D} .

Although general nondiagonal rescaling could yield the projection much more costly [6], for diagonal rescaling considered in our case, the following theorem shows that this projection can be computed by solving an equivalent root-finding problem.

Theorem 1. *The projection of (t, \mathbf{x}) onto rescaled cone $\mathbf{D}\mathcal{K}_{\text{soc}}^{n+1}$ is given as follows.*

1. If $t \leq 0$ and $\|\hat{\mathbf{D}}\mathbf{x}\| \leq -t$, the projection $\text{Proj}_{\mathbf{D}\mathcal{K}_{\text{soc}}^{n+1}} \{(t, \mathbf{x})\} = (0, \mathbf{0})$.

2. If $\|\hat{\mathbf{D}}^{-1}\mathbf{x}\| \leq t$, then $\text{Proj}_{\mathcal{K}_{\text{soc}}^{n+1}} \{(t, \mathbf{x})\} = (t, \mathbf{x})$.
3. If $t = 0$ and $\mathbf{x} \neq \mathbf{0}$, then $\text{Proj}_{\mathcal{K}_{\text{soc}}^{n+1}} \{(t, \mathbf{x})\} = \left(\|(\hat{\mathbf{D}} + \hat{\mathbf{D}}^{-1})^{-1}\mathbf{x}\|, (\mathbf{I}_{n \times n} + \hat{\mathbf{D}}^{-2})^{-1}\mathbf{x} \right)$.
4. Otherwise, if $\|\hat{\mathbf{D}}^{-1}\mathbf{x}\| > t$, then let $\lambda > 0$ be the solution of the following system of λ :

$$\sum_{i=2}^{n+1} \left(\frac{\hat{\mathbf{d}}_i^{-1}}{1 + 2\lambda \hat{\mathbf{d}}_i^{-2}} \right)^2 \mathbf{x}_i^2 - \frac{t^2}{(1 - 2\lambda)^2} = 0, \quad \frac{t}{(1 - 2\lambda)} > 0.$$

Then the projection is given by $\text{Proj}_{\mathcal{K}_{\text{soc}}^{n+1}} \{(t, \mathbf{x})\} = \left((1 - 2\lambda)^{-1}t, (\mathbf{I} + 2\lambda \hat{\mathbf{D}}^{-2})^{-1}\mathbf{x} \right)$.

In the PDCS implementation, the fourth case is handled using a root-finding routine based on a bijection method.

Proof of Theorem 1. First of all, we consider the simplest case of (s, \mathbf{y}) —when it is the degenerate solution $(0, \mathbf{0})$. It should be noted that the projection onto a convex cone $\hat{\mathbf{D}}\mathcal{K}_{\text{soc}}^{n+1}$ is $(0, \mathbf{0})$ if and only if $-(t, \mathbf{x})$ lies in the dual cone of $\hat{\mathbf{D}}\mathcal{K}_{\text{soc}}^{n+1}$. Because $(\hat{\mathbf{D}}\mathcal{K}_{\text{soc}}^{n+1})^* = \hat{\mathbf{D}}^{-1}(\mathcal{K}_{\text{soc}}^{n+1})^* = \hat{\mathbf{D}}^{-1}(\mathcal{K}_{\text{soc}}^{n+1})^*$, it implies that when $\|\hat{\mathbf{D}}\mathbf{x}\| \leq -t$, the projection (s, \mathbf{y}) is $(0, \mathbf{0})$. This proves the first case.

Now we introduce the multipliers $\lambda \geq 0$ and $\mu \geq 0$ for the two constraints of (11), then the Lagrangian is $\mathcal{L}(\mathbf{y}, s; \lambda, \mu) = \frac{1}{2}\|\mathbf{y} - \mathbf{x}\|^2 + \frac{1}{2}(s - t)^2 + \lambda(\|\hat{\mathbf{D}}^{-1}\mathbf{y}\|^2 - s^2) + \mu(-s)$. Thus, the KKT condition of (11) is as follows:

$$\|\hat{\mathbf{D}}^{-1}\mathbf{y}\|^2 - s^2 \leq 0, \quad s \geq 0, \quad \lambda \geq 0, \quad \mu \geq 0 \quad (12)$$

$$\mathbf{y} - \mathbf{x} + 2\lambda\hat{\mathbf{D}}^{-2}\mathbf{y} = 0, \quad (s - t) - 2\lambda s - \mu = 0 \quad (13)$$

$$\lambda(\|\hat{\mathbf{D}}^{-1}\mathbf{y}\|^2 - s^2) = 0, \quad \mu s = 0 \quad (14)$$

It should be noted that Slater's condition holds for (11) as there exist strictly feasible solutions, any nonzero (s, \mathbf{y}) satisfying (12), (13) and (14) is an optimal solution pair for (11).

Let us start from the simplest case. If (t, \mathbf{x}) is already in the rescaled cone, i.e., $\|\hat{\mathbf{D}}^{-1}\mathbf{x}\|^2 \leq t^2$, then $(s, \mathbf{y}) = (t, \mathbf{x})$ is an optimal solution for (11) because it is feasible and has the smallest possible objective value 0. This proves the second case.

Now we consider the other case $\|\hat{\mathbf{D}}^{-1}\mathbf{x}\|^2 > t^2$. Since (t, \mathbf{x}) is not in the rescaled cone, the projected solution (s, \mathbf{y}) must lie in the boundary of the cone. In other words, $\|\hat{\mathbf{D}}^{-1}\mathbf{y}\| = s$. If $t = 0$, then the optimality conditions (12), (13) and (14) become

$$(\mathbf{y} - \mathbf{x}) + 2\lambda\hat{\mathbf{D}}^{-2}\mathbf{y} = 0, \quad s - 2\lambda s = \mu, \quad s\mu = 0, \quad \|\hat{\mathbf{D}}^{-1}\mathbf{y}\|^2 = s^2, \quad s \geq 0, \quad \lambda \geq 0, \quad \mu \geq 0. \quad (15)$$

One can observe that in this case

$$\mathbf{y} = (\mathbf{I}_{n \times n} + \hat{\mathbf{D}}^{-2})^{-1}\mathbf{x}, \quad s = \|(\hat{\mathbf{D}} + \hat{\mathbf{D}}^{-1})^{-1}\mathbf{x}\|, \quad \lambda = \frac{1}{2}, \quad \mu = 0 \quad (16)$$

satisfy the above system. Therefore, when $t = 0$ and $\|\hat{\mathbf{D}}^{-1}\mathbf{x}\| > 0$, (16) gives the solution s and \mathbf{y}

for (11). This proves the third case.

If $t > 0$, let $\mu = 0$ and then the optimality conditions (12), (13) and (14) become

$$(\mathbf{y} - \mathbf{x}) + 2\lambda\hat{\mathbf{D}}^{-2}\mathbf{y} = 0, \quad (1 - 2\lambda)s = t, \quad \|\hat{\mathbf{D}}^{-1}\mathbf{y}\|^2 = s^2, \quad s \geq 0, \quad \lambda \geq 0. \quad (17)$$

If there exist \mathbf{y} , s and $\lambda \in (0, \frac{1}{2})$ satisfying (17), then \mathbf{y} and s can be computed by the first and second equations:

$$\mathbf{y} = (\mathbf{I} + 2\lambda\hat{\mathbf{D}}^{-2})^{-1}\mathbf{x}, \quad s = (1 - 2\lambda)^{-1}t \geq 0 \quad (18)$$

Substituting them into the third equation yields:

$$\underbrace{\|(\hat{\mathbf{D}} + 2\lambda\hat{\mathbf{D}}^{-1})^{-1}\mathbf{x}\|^2 - (1 - 2\lambda)^{-2}t^2}_{\text{Denoetd by } f(\lambda)} = 0. \quad (19)$$

Note that there must exist a root $\lambda \in (0, \frac{1}{2})$ of the above equation $f(\lambda) = 0$ because f is continuous on $(0, \frac{1}{2})$, while $\lim_{\lambda \rightarrow 0+} f(\lambda) > 0$ (since $\|\hat{\mathbf{D}}^{-1}\mathbf{x}\|^2 > t^2$) and $\lim_{\lambda \rightarrow \frac{1}{2}} f(\lambda) < 0$ (since $t > 0$). Therefore, let λ be a root of (19) and then (18) gives the solution \mathbf{y} and s .

Similarly, if $t < 0$ and $\|\hat{\mathbf{D}}\mathbf{x}\| > -t$ (the cases $\|\hat{\mathbf{D}}\mathbf{x}\| \leq -t$ has been discussed in the begining), then there exists $\lambda > \frac{1}{2}$ that is a root of $f(\lambda) = 0$. The existence of such a root is due to $\|\hat{\mathbf{D}}\mathbf{x}\| > -t$. Then (18) gives the solution \mathbf{y} and s based using the root λ . Now the fourth case is proven. \square

Projection onto rescaled exponential cones. If a vector can be expressed as the sum of two orthogonal components belonging to a primal-polar pair of non-empty closed convex cones, then these components correspond to the respective projections of the point onto each cone [47]. Applying this result into the projection of a point \mathbf{v}_0 onto an exponential cone with diagonal rescaling $\mathbf{D} = \begin{pmatrix} d_r & & \\ & d_s & \\ & & d_t \end{pmatrix}$, the projection problem can thus be characterized by solving the following system in terms of \mathbf{v}_p and \mathbf{v}_d :

$$\mathbf{v}_0 = \mathbf{v}_p + \mathbf{v}_d, \quad \mathbf{v}_p \in \mathbf{D}\mathcal{K}_{\text{exp}}, \quad \mathbf{v}_d \in -\mathbf{D}^{-1}\mathcal{K}_{\text{exp}}^*, \quad \mathbf{v}_p^\top \mathbf{v}_d = 0, \quad (20)$$

where $-\mathbf{D}^{-1}\mathcal{K}_{\text{exp}}^* := \left\{ (r, s, t) \in \mathbb{R}^3 \mid r > 0, (-\exp(1))d_t t \geq d_r r \exp\left(\frac{d_s s}{d_r r}\right) \right\} \cup \{(r, s, t) \in \mathbb{R}^3 \mid r = 0, t \leq 0, s \leq 0\}$. In particular, \mathbf{v}_p is $\text{Proj}_{\mathbf{D}\mathcal{K}_{\text{exp}}}(\mathbf{v}_0)$ and $-\mathbf{v}_d$ is $\text{Proj}_{\mathbf{D}^{-1}\mathcal{K}_{\text{exp}}^*}(\mathbf{v}_0)$.

It could be proven that the solution pair \mathbf{v}_p and \mathbf{v}_d from (20) can be parameterized by a scalar. Therefore, the projection problem can also be reduced to a root-finding problem that can be solved by a bijection search method. We defer the proof of this result and the implementation details of the projection to Appendix B.

4 cuPDCS: A PDCS Implementation with GPU Enhancements

In this section, we present the design and implementation of PDCS optimized for better exploiting GPU architectures. We name this GPU implementation as cuPDCS. The solver is available at

<https://github.com/ZikaiXiong/PDCS>.

As demonstrated in previous sections, the primary computational bottlenecks of PDCS are matrix–vector multiplications and projections onto cones. While matrix–vector multiplications are already well-optimized on GPUs (see, e.g., [5]), projections onto cones remain comparatively under-optimized. (An exception is the LP cone, for which the projection is an elementwise comparison and thus straightforward to parallelize.) Consequently, developing an efficient projection strategy is essential for achieving overall performance gains in our cuPDCS solver.

We first briefly review the hierarchical organization of GPU parallel computing, which comprises three levels of execution granularity: grid, block, and thread (Figure 1). Upon dispatch to the GPU, each workload is organized into a single grid consisting of multiple blocks; each block contains numerous threads that share block-level (shared) memory and can synchronize their execution. Accordingly, it is crucial to allocate computational resources properly. Moreover, empirical evidence indicates that frequent data transfers between the CPU and GPU result in significant overhead. This is a primary reason why existing GPU solvers (such as [40, 44] et al.) almost all emphasize executing the majority of computations mostly on the GPU. Consequently, a fundamental design principle for projection operators is to reduce as much as possible data transfers between the CPU and GPU while maximizing the proportion of computations executed on the GPU. In the case of multi-cone projection, it is also essential to allocate computational resources in a manner that enables all cone projections to be executed in parallel. Recall that, as indicated in (4), cone projections can be carried out by separately projecting onto rescaled disciplined cones. As discussed in Section 3.5, projections onto second-order and exponential cones can be reformulated as root-finding problems that typically involve a few vector inner products and scalar multiplications.

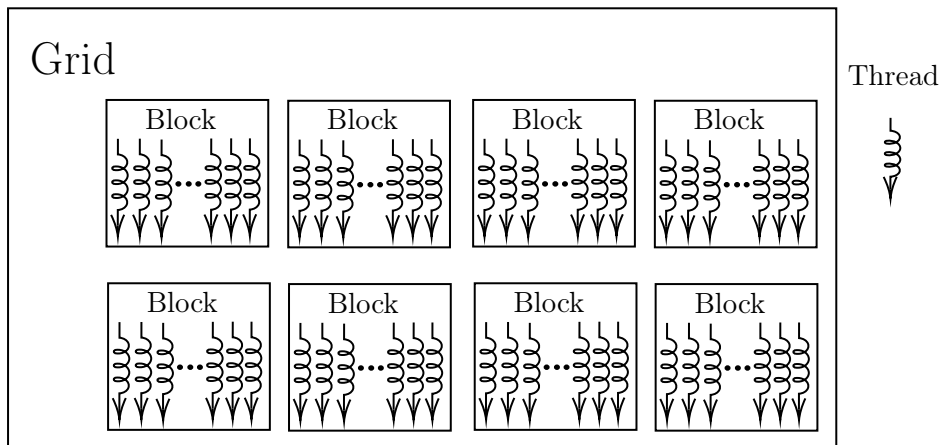


Figure 1: Illustration of the GPU architecture.

In our GPU implementation of PDCS, we employ three parallel computing strategies:

1. **Grid-wise.** Assign the entire grid to execute each cone projection sequentially. Vector inner products are computed using the cuBLAS library, which delivers high-performance capability for individual operations. However, each cuBLAS call also incurs significant launch and resource-allocation overhead.
2. **Block-wise.** Assign one disciplined cone projection to each CUDA block. This approach amortizes the kernel-launch overhead by simultaneously processing many cones within a single kernel invocation.
3. **Thread-wise.** Assign one disciplined cone projection to each CUDA thread. This strategy removes nearly all synchronization and kernel-launch overhead, allowing simultaneous processing of a large number of tasks by distributing them across individual threads.

A distinguishing feature of the projection phase is that the number, dimension, and type of individual disciplined cones can vary substantially. Consequently, no single parallelization strategy can be expected to perform optimally across all cone types or configurations. For instance, consider the task of projecting a randomly generated vector $\mathbb{R}^{m \times (d+1)}$ onto a multi-block second-order cone $\mathcal{K} := \mathcal{K}_{\text{soc}}^{d+1} \times \mathcal{K}_{\text{soc}}^{d+1} \times \dots \times \mathcal{K}_{\text{soc}}^{d+1}$ where there are m second-order cone blocks. In our experiments, we fix the dimension d of each cone as $d = \left\lceil \frac{1.2 \times 10^9}{m} \right\rceil$, thus ensuring that the total dimensionality of the cone remains at least 1.2×10^9 . Figure 2 compares the performance of the three proposed strategies—grid-wise (one grid per projection), block-wise (one block per projection), and thread-wise (one thread per projection)—under this configuration. In this test, a time limit of 15 seconds is imposed, and we report the average runtime along with the standard deviation (indicated by the shaded region) over 10 independent trials. Note that the CPU implementation of these projections always requires more than 15 seconds; hence, its data points are represented by a horizontal dotted line at 15 seconds.

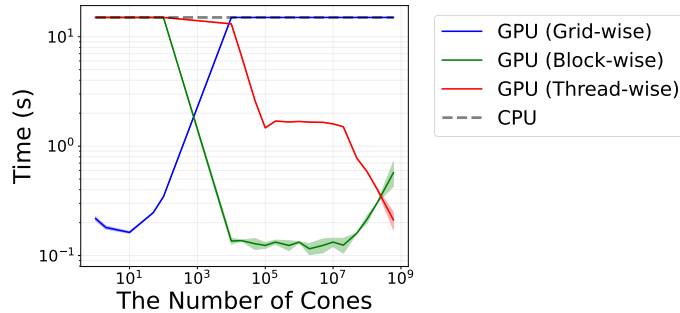


Figure 2: Runtime of projections onto second-order cones

Intuitively, the grid-wise strategy benefits from the highly optimized norm computations provided by the cuBLAS library, rendering it particularly effective for a small number of high-dimensional tasks. However, this strategy suffers when addressing a large number of small-dimension tasks, as each cuBLAS function call incurs non-negligible overhead that accumulates significantly across many

projections. In contrast, the block-wise approach, which effectively utilizes shared memory to perform in-block reductions, is ideally suited for a moderate number of tasks with moderate dimensions. Finally, the thread-wise method may become the best when the workload consists of a very large number of very low-dimensional tasks, as each small cone projection can be efficiently handled by an individual thread, and the overall massive parallelism is fully exploited.

When m (the number of cones) is very small (i.e., each cone is high-dimensional), the grid-wise strategy performs best. As m grows and d becomes moderate, the block-wise strategy becomes more efficient. Ultimately, when m is extremely large (yielding many small cones), the thread-wise approach is the best, since a single thread is sufficient for handling the small cone projection and the large number of threads provides high parallelism. Note that we have a time limit of 15 seconds for the projection task, and both the thread-wise and block-wise strategies exceed the threshold for a small number of high-dimensional cones, whereas the grid-wise strategy exceeds the threshold as the number of cones increases.

Another key factor in resource allocation is the computational cost associated with different cone types. For the zero and nonnegative cones, the projection requires only simple elementwise comparisons (and, for the nonnegative cone, scalar clamping). These inexpensive operations have negligible synchronization or overhead. Projection onto the exponential cone, by solving the conditions in (26), likewise consists primarily of elementwise comparisons and scalar multiplications, making it well-suited for thread-level parallelism. Consequently, for these three cone types, we assign one GPU thread per cone, thereby minimizing synchronization overhead.

In contrast, projection onto a second-order cone with diagonal rescaling (Theorem 1) reduces to solving a univariate root-finding problem that involves both elementwise products and a Euclidean norm calculation. While the elementwise products can be handled in parallel, the norm computation necessitates a reduction (i.e., summation), which requires synchronization. To balance throughput and synchronization costs, we implement reduction at three distinct levels. At the grid level, we directly leverage the cuBLAS library; at the block level, reduction is conducted using shared memory; and at the thread level, we perform serial addition. These three strategies correspond to the methods we previously proposed and are aimed to ensuring efficiency for second-order cone projections under varying scenarios.

Both the block-wise and thread-wise strategies avoid repeated CPU–GPU data transfers and the overhead associated with multiple cuBLAS calls by performing the entire projection operation within a single kernel launch. By selecting the number of blocks (in the block-wise strategy) or threads (in the thread-wise approach) based on available GPU resources, we can execute projections for all cones in a multi-cone structure concurrently. This approach increases hardware utilization, and leads to more efficient projections for large-scale instances. Table 2 summarizes the projection strategies for different cone types.

Finally, we examine the effectiveness of these strategies on exponential-cone projections in Figure 3 by projecting a randomly generated vector to a multi-block exponential cone. We compare the GPU-based, thread-wise strategy to a CPU-based implementation as the number of cones varies.

Table 2: Projection strategies for different cone types

Cone Type	Thread-wise	Block-wise	Grid-wise
Zero Cone	✓	✗	✗
Nonnegative Cone	✓	✗	✗
Second-order Cone	✓	✓	✓
Exponential Cone	✓	✗	✗

Similar to Figure 2, Figure 3 displays the mean projection time over ten runs, with the shaded region representing the corresponding standard deviation. The results demonstrate that the massive parallelism of the GPU provides significant speedups, and the performance gap between the GPU- and CPU-based implementations widens with increasing numbers of cones.

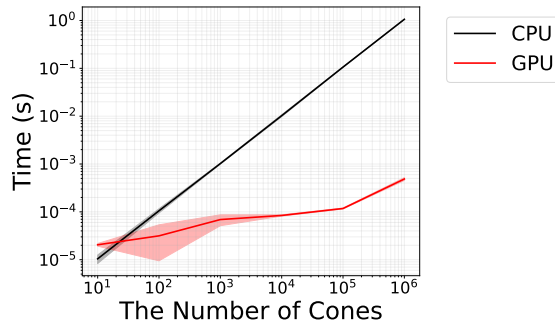


Figure 3: Projections onto exponential cones

5 Numerical experiments

In this section, we evaluate the performance of our solver on a diverse set of problem instances, comparing it with several other state-of-the-art conic solvers that use either first-order methods or interior-point methods (barrier methods):

- **SCS** [49] and **ABIP** [17]: Open-source, ADMM-based conic solvers. SCS provides three variants: CPU-direct, CPU-indirect, and GPU-indirect. The “direct” and “indirect” refer to whether a direct method (using matrix factorizations) or an iterative method (using the conjugate gradient method) is employed to solve the inner linear systems.
- **CuClaravel** [14]: An open-source solver implementing an interior-point method for conic problems with GPU acceleration. It uses the cuDSS library to solve the linear systems on the GPU via matrix factorizations.
- **MOSEK** [3] and **COPT** [24]: State-of-the-art commercial interior-point method based solvers.

The methods that do not require matrix factorizations or require only a single matrix factorization are classified as first-order methods. They are SCS (either direct or indirect), ABIP and PDCS

(including its GPU implementation cuPDCS). The other solvers are essentially based on interior-point methods (also known as barrier methods). They are CuClarelab, MOSEK and COPT. For certain problem instances, the presolve capabilities of the commercial solvers can detect structural properties, thereby significantly reducing problem complexity and potentially offering a computational advantage. We denote versions of COPT and MOSEK with presolve enabled as COPT* and MOSEK*, respectively, and the versions without presolve as COPT and MOSEK. In Sections 5.2, 5.3, and 5.4, we will compare these variations in greater detail.

This comparison in this section allows us to assess the relative strengths and shortcomings of PDCS and cuPDCS across various problem regimes. We organize the experiments as follows. Section 5.1 evaluates performance on the CBLIB dataset, a small-scale classical conic program dataset. In Section 5.2, we consider the Fisher market equilibrium problem, a conic programming problem involving the exponential cone. Section 5.3 focuses on solving a large-scale Lasso problem, which can be reformulated into a second-order cone problem. Last, in Section 5.4, we consider multi-period portfolio optimization, which is a conic programming problem with multiple second-order cones.

For testing case in Section 5.2, 5.3 and 5.4, we set time limit as 2 hours for 10^{-3} tolerance and 5 hours for 10^{-6} tolerance. All GPU experiments are conducted on an NVIDIA H100 with 80 GB of VRAM, running on a cluster equipped with an Intel Xeon Platinum 8468 CPU. All CPU benchmarks are performed on a Mac mini M2 Pro with 32 GB of RAM.

Because each solver adopts different formulations and methodologies, their actual built-in termination criteria can vary even if setting the same tolerance requirement. Moreover, some solvers keep their termination criteria private. For these reasons, there is no uniform convergence standard across the solvers we evaluated, but we attempt to document and summarize the known termination criteria for these solvers in Appendix D. As for PDCS and cuPDCS, we assess primal and dual feasibility, as well as primal–dual optimality, with the following metrics derived from (P) and (D). We define the primal feasibility error, dual feasibility error, and primal–dual gap as:

$$\begin{aligned}
\text{err}_p(\mathbf{x}) &:= \frac{\|(\mathbf{G}\mathbf{x} - \mathbf{h}) - \text{Proj}_{\mathcal{K}_d^*}\{\mathbf{G}\mathbf{x} - \mathbf{h}\}\|_\infty}{1 + \max\{\|\mathbf{h}\|_\infty, \|\mathbf{G}\mathbf{x}\|_\infty, \|\text{Proj}_{\mathcal{K}_d^*}\{\mathbf{G}\mathbf{x} - \mathbf{h}\}\|_\infty\}} , \\
\text{err}_d(\boldsymbol{\lambda}_1, \boldsymbol{\lambda}_2) &:= \frac{\max\{\|\boldsymbol{\lambda}_1 - \text{Proj}_{\Lambda}\{\boldsymbol{\lambda}_1\}\|_\infty, \|\boldsymbol{\lambda}_2 - \text{Proj}_{\mathcal{K}_p^*}\{\boldsymbol{\lambda}_2\}\|_\infty\}}{1 + \max\{\|\mathbf{c}\|_\infty, \|\mathbf{G}^\top \mathbf{y}\|_\infty\}} , \\
\text{err}_{\text{gap}}(\mathbf{x}, \boldsymbol{\lambda}_1, \boldsymbol{\lambda}_2) &:= \frac{|\langle \mathbf{c}, \mathbf{x} \rangle - (\mathbf{y}^\top \mathbf{h} + \mathbf{l}^\top \boldsymbol{\lambda}_1^+ + \mathbf{u}^\top \boldsymbol{\lambda}_1^-)|}{1 + \max\{|\langle \mathbf{c}, \mathbf{x} \rangle|, |\mathbf{y}^\top \mathbf{h} + \mathbf{l}^\top \boldsymbol{\lambda}_1^+ + \mathbf{u}^\top \boldsymbol{\lambda}_1^-|\}} .
\end{aligned} \tag{21}$$

Our solver terminates once all three of these criteria fall below a specified tolerance, which is usually either 10^{-3} or 10^{-6} .

In order to comprehensively compare the runtime of different solvers across multiple instances, we use the shifted geometric mean (SGM) [46] defined as follows:

$$\text{SGM}(k) = \left[\prod_{i=1}^N (t_i + k) \right]^{1/N} - k ,$$

where t_i is the time (in seconds) for solver i on problem i , and k is a positive shift. The SGM is able to mitigate the potentially significant influence of tiny runtimes of only a few instances on the overall geometric mean. If a solver fails to solve a given instance, we assign t_i to be the maximum allowable time (e.g., the time limit).

5.1 Relaxtion of Problems from the CBLIB Dataset

CBLIB¹ is a public dataset of mixed-integer conic programming problems collected from real-world applications [21]. We run our experiments on the instances with LP cones, second-order cones, and exponential cones. In line with standard practice for solving such problems, we first use COPT to apply presolve and subsequently relax all integer constraints, thereby producing two refined subsets: (1) 1,943 problems that do not involve exponential cones, and (2) 157 problems that include exponential cones.

For the subset without exponential cones, we further categorize problem instances as small-, medium-, and large-scale based on the number of non-zeros in the constraint matrix, using thresholds of 50,000 and 500,000. As a result, the dataset comprises 1,641 small-scale, 220 medium-scale and 82 large-scale problem instances. In spite of this classification, it should be noted that almost all of these problems are relatively small in scale so the barrier method-based solvers and the SCS(direct) would not reach computational bottlenecks and can easily conduct the matrix factorization. We start with this dataset to give an overview of the performance of PDCS on small-scale problems. All experiments in this benchmark are executed with a one-hour time limit and a termination tolerance of 10^{-6} .

Tables 3 and 4 summarize the results for these two categories of problems. Among the first-order methods, SCS(indirect) is the fastest for small-scale problems and the problems with exponential cones. Our cuPDCS is faster for the medium-scale and large-scale problems without exponential cones. Since all these problems are relatively still small-scale, the barrier methods all perform far better than first-order methods.

Both the CPU-based version of our solver (denoted by PDCS) and its GPU-enhanced implementation (denoted by cuPDCS) exhibit strong numerical stability, solving nearly as many instances as the commercial solver COPT. However, the CPU version occasionally struggles with more challenging instances, primarily due to the limited parallelism in projection operations and matrix-vector multiplications. In contrast, the GPU implementation, cuPDCS, enables more iterations within the allotted time and successfully solves some instances that are otherwise too difficult for the CPU version. Overall, cuPDCS demonstrates a substantial performance advantage over its CPU counterpart.

Among all these methods, only SCS(indirect), and PDCS along with cuPDCS are matrix-free methods. The computational bottleneck of matrix-free methods lies in the sparse matrix-vector products, so we also compare the number of matrix-vector products required for cuPDCS and SCS(indirect) to solve a particular number of problems. Figure 4 shows the number of matrix-vector

¹<https://cblib.zib.de/download/all/> Accessed: 2025-04-06.

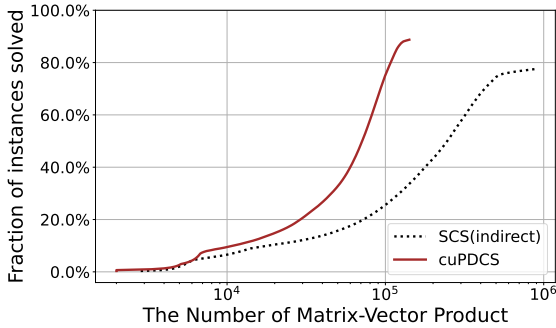
Table 3: Conic Program Problems without Exponential Cones

		Small(1641)		Medium(220)		Large(82)		Total(1943)	
		SGM(10)	count	SGM(10)	count	SGM(10)	count	SGM(10)	count
First-order methods	ABIP	3.66	1622	1342.77	84	3458.00	2	19.04	1708
	SCS(direct)	0.59	1636	54.98	213	463.21	58	5.26	1907
	SCS(indirect)	3.31	1638	231.68	188	1856.58	46	12.77	1872
	PDCS	2.78	1640	160.64	208	1602.14	53	11.02	1901
	cuPDCS	2.91	1640	44.95	211	312.65	57	7.43	1908
Barrier methods	CuClarabel	0.15	1640	1.32	219	46.17	61	1.05	1920
	COPT*	0.08	1639	2.03	215	53.76	58	1.12	1912
	MOSEK*	0.05	1640	2.34	214	6.21	81	0.49	1935

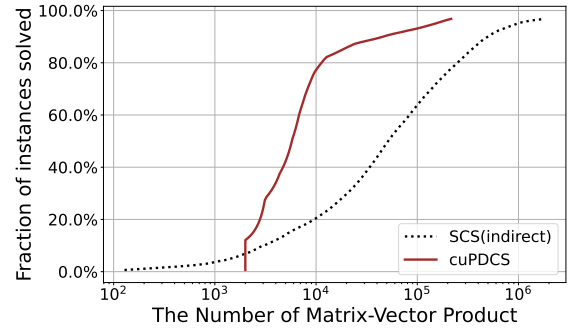
Table 4: Conic Program Problems with Exponential Cones

First-order methods					Barrier methods		
	SCS(direct)	SCS(indirect)	PDCS	cuPDCS	CuClarabel	COPT*	MOSEK*
SGM(10)	6.07	19.98	17.43	12.04	0.87	0.13	5.19
count	152	152	152	155	156	157	146

products and the corresponding fraction of instances solved within this number. Notably, when we compare the number of matrix-vector products needed to solve 60% of the problem instances, we see that cuPDCS requires only about one-fifth to one-tenth as many matrix-vector products as the indirect SCS. Since cuPDCS follows the PDCS algorithm, we can conclude that, even if not implemented on a GPU, PDCS still requires fewer iterations than the other matrix-free solver, SCS(indirect). This advantage is not clearly reflected in the runtime reported in Table 3 because the actual runtime significantly depends on implementation details and programming language. In particular, for small-scale problems, a substantial amount of time is consumed by fixed overheads.



(a) Medium- and large-scale conic program problems without exponential cones



(b) Conic program problems with exponential cones

Figure 4: Performance of cuPDCS and SCS(indirect) in terms of the number of matrix-vector products.

Among the barrier methods, MOSEK* consistently demonstrates advantages over other solvers for conic programs without exponential cones. However, for problems involving exponential cones,

MOSEK* frequently fails to meet the necessary solution tolerance, resulting in a “SLOW_PROGRESS” status. In our analysis, all such instances are regarded as failures, irrespective of whether the time limit is reached. Additionally, our tolerance settings differ from those in [17], and ABIP’s difficulty in achieving high-precision solutions under our stricter tolerance results in seemingly poorer performance compared to what is reported in Table 13 of [17].

It should be emphasized that the problems in the CBLIB dataset are relatively small in scale. For these problems, solving the matrix factorizations and the corresponding linear systems remains accessible. Hence, the SCS with direct factorizations implemented on CPUs appears to be the best first-order method, while all interior-point methods significantly outperform first-order methods. However, as the dimension of the problem instance increases, SCS(direct) and all interior-point methods face greater challenges and become considerably slower. In the following sections, we present the experiments on larger-scale problem instances.

5.2 Fisher Market Equilibrium Problem

The first class of conic problem instances we are testing on is the Fisher Equilibrium Problem [18, 64], an important optimization problem arising in economics. It is formulated as follows [18]:

$$\min_{\mathbf{x} \in \mathbb{R}^{m \times n}} - \sum_{i \in [m]} \mathbf{w}_i \left(\log \left(\sum_{j \in [n]} \mathbf{U}_{ij} \mathbf{x}_{ij} \right) \right) \quad \text{s. t.} \quad \sum_{i \in [m]} \mathbf{x}_{ij} = \mathbf{b}_j, \quad \mathbf{x}_{ij} \geq 0, \quad (22)$$

where m is the number of buyers, n is the number of goods, $\mathbf{w} \in \mathbb{R}^m$, $\mathbf{U} \in \mathbb{R}^{m \times n}$. The vector $\mathbf{w} \in \mathbb{R}^m$ represents the monetary endowment of each buyer, $\mathbf{U} \in \mathbb{R}^{m \times n}$ denotes the utility of each buyer for each good and the j -th entry of \mathbf{b} denotes the overall amount of goods j . In this formulation, each buyer i allocates their budget \mathbf{w} to maximize their utility, while each seller j offers a good for sale. An equilibrium is reached when goods are priced so that every buyer acquires an optimal bundle and the market clears—meaning all budgets are spent and all goods are sold.

This problem can be equivalently formulated as a conic program problem with exponential cones. We formulate it as a standard conic problem (see the specific formulation in Appendix C) and compare various solvers (excluding ABIP as it is not applicable) under two levels of solution accuracy: low accuracy (10^{-3}) and high accuracy (10^{-6}). The results are summarized in Table 5. In the experiments, we consider some different dimension choices of m and n for matrix \mathbf{U} while maintaining a constant sparsity level of 0.2. Each nonzero entry of \mathbf{w} and \mathbf{U} is sampled independently from the uniform distribution $U[0, 1]$, and we set $\mathbf{b}_j = 0.25$ for all $j \in [n]$. The time limits are set to 2 hours for the low-accuracy tests and 5 hours for the high-accuracy tests. The first three columns m , n and nnz of Table 5 denote the number of rows, the number of columns, and the number of nonzero entries of \mathbf{U} .

As shown in Table 5, cuPDCS consistently outperforms the other matrix-free GPU-enhanced solver, SCS(GPU). Although both solvers utilize GPU, SCS(GPU) is significantly slower. This is primarily because SCS(GPU) is a GPU implementation of SCS(indirect), which typically requires

Table 5: Experiments on Fisher market equilibrium problems.

m	n	nnz	Without Presolve					With Presolve	
			cuPDCS	SCS(GPU)	CuClarabel	COPT	MOSEK	COPT*	MOSEK*
10 ⁻³									
1.0E+02	5.0E+03	1.0E+05	1.5E+01	f	1.0E+01	2.6E+00	1.0E+00	2.8E+00	4.2E-01
1.0E+05	1.0E+03	2.0E+07	4.6E+02	f	f	f	2.5E+03	f	1.5E+02
1.5E+05	1.0E+03	3.0E+07	4.3E+02	f	f	f	f	f	2.5E+02
2.0E+05	1.0E+03	4.0E+07	1.1E+03	f	f	f	f	f	3.9E+03
2.5E+05	1.0E+03	5.0E+07	1.4E+03	f	f	f	f	f	6.4E+03
2.8E+05	1.0E+03	5.5E+07	1.6E+03	f	f	f	f	f	f
10 ⁻⁶									
1.0E+02	5.0E+03	1.0E+05	3.7E+01	1.2E+04	1.2E+01	2.8E+00	1.1E+00	3.0E+00	4.2E-01
1.0E+05	1.0E+03	2.0E+07	1.8E+03	f	f	f	2.7E+03	f	1.8E+02
1.5E+05	1.0E+03	3.0E+07	2.8E+03	f	f	f	f	f	2.9E+02
2.0E+05	1.0E+03	4.0E+07	4.2E+03	f	f	f	f	f	4.0E+03
2.5E+05	1.0E+03	5.0E+07	5.7E+03	f	f	f	f	f	6.5E+03
2.8E+05	1.0E+03	5.5E+07	6.2E+03	f	f	f	f	f	7.7E+03

Note. Entries marked “f” indicate failure due to exceeding the time limit or returning errors. Bold entries indicate the best runtime among all solvers for each row. Shaded cells highlight the best-performing method on the original problem (without presolve).

more iterations to converge than cuPDCS. Moreover, SCS(GPU) uses the GPU only to accelerate the iterative method for solving the linear system, while the rest of the algorithm remains implemented on CPU. This design results in substantial data transfer between the CPU and GPU, which incurs significant overhead and slows down the overall performance. In spite of this, SCS(GPU) is still faster than its two CPU versions, SCS(indirect) and SCS(direct).

Even when compared to interior-point methods such as COPT and MOSEK, cuPDCS performs competitively—often outperforming them on problem instances where \mathbf{U} contains more than 2×10^7 nonzero elements. Although CuClarabel is a GPU-accelerated interior-point solver, its performance is generally closer to that of COPT and MOSEK than to cuPDCS, suggesting that classic interior-point methods benefit less from GPU acceleration than first-order methods. It is also worth noting that cuPDCS is more sensitive to accuracy requirements than interior-point solvers. When the target tolerance tightens from 10^{-3} to 10^{-6} , the runtime of cuPDCS increases significantly, while the runtimes of interior-point methods remain relatively stable. This indicates that computing high-accuracy solutions is more challenging for cuPDCS.

The presolve function in commercial solvers can significantly affect performance. For MOSEK, presolve leads to improved robustness and faster runtimes. MOSEK* performs substantially better than its non-presolved counterpart. Conversely, for COPT, presolve leads to a slight performance degradation in our experiments. These differences arise from the ability of presolve to exploit matrix structure and reduce the cost of matrix factorizations, though the benefits are not always guaranteed. When only comparing algorithm performance on the original problems (without presolve), cuPDCS performs the best on all problems but the smallest-scale problem, as indicated by the shaded cells.

To further illustrate the scalability of cuPDCS, Figure 5 compares its performance against

MOSEK and MOSEK*. The plots show runtime as a function of problem size, measured by the number of nonzero elements in \mathbf{U} . In the low-accuracy setting, cuPDCS enjoys a substantial speed advantage over MOSEK, and this advantage becomes more pronounced as the problem size increases. Moreover, regardless of the target tolerance, when the number of nonzeros exceeds approximately 4×10^7 , the runtime of MOSEK* grows sharply, whereas cuPDCS maintains better scalability, showcasing the benefits of GPU-accelerated first-order methods for solving large-scale conic programs.

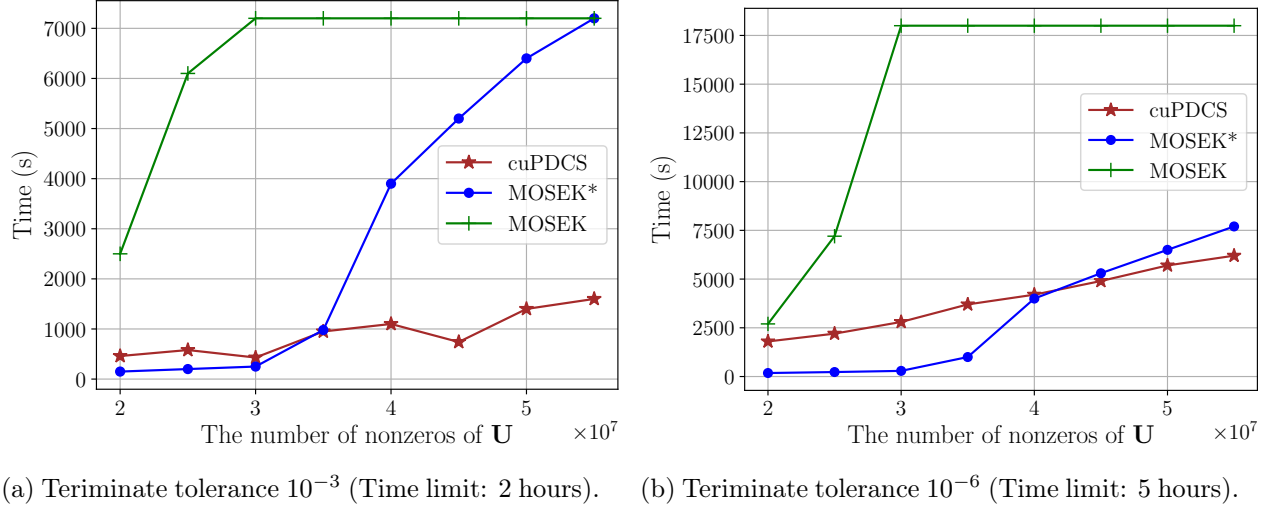


Figure 5: The performance of cuPDCS and MOSEK.

5.3 Lasso Problem

The Lasso problem is a fundamental optimization model in statistical learning that integrates variable selection and regularization to improve both prediction accuracy and model interpretability [57]:

$$\min_{\mathbf{x} \in \mathbb{R}^n} \|\mathbf{A}\mathbf{x} - \mathbf{b}\|^2 + \lambda \|\mathbf{x}\|_1,$$

where matrix $\mathbf{A} \in \mathbb{R}^{m \times n}$, $\mathbf{b} \in \mathbb{R}^m$ and $\lambda > 0$ is the regularization parameter.

We generate a family of synthetic Lasso problem instances following the experimental setting used for ABIP in [17]. Specifically, the matrix $\mathbf{A} \in \mathbb{R}^{m \times n}$ is generated with a fixed sparsity level of 10^{-4} , where each nonzero entry is drawn independently from the uniform distribution, i.e., $\mathbf{A}_{ij} \sim U[0, 1]$ for all i and j . The label vector \mathbf{b} is then generated by $\mathbf{b} = \mathbf{A}\tilde{\mathbf{x}} + 10^{-6} \cdot \mathbf{1}$, where $\tilde{\mathbf{x}} \in \mathbb{R}^n$ has entries drawn independently from the standard normal distribution, and half of its components are randomly set to zero. The vector $\mathbf{1}$ denotes the all-ones vector. The regularization parameter λ is set to $\|\mathbf{A}^\top \mathbf{b}\|_\infty$, same as [17].

By decomposing the decision variable \mathbf{x} into its positive and negative parts, the problem can be equivalently reformulated as an SOCP. The complete SOCP formulation is provided in Appendix C.2. We compare various solvers under two levels of solution accuracy: low accuracy (10^{-3}) and high accuracy (10^{-6}). The results are summarized in Table 6. The first three columns m , n

and nnz denote the number of rows, the number of columns, and the number of nonzero entries of \mathbf{A} .

Table 6: Experiments on Lasso problems.

m	n	nnz	Without Presolve					With Presolve		
			cuPDCS	SCS(GPU)	ABIP	CuClarabel	COPT	MOSEK	COPT*	MOSEK*
10 ⁻³										
1.0E+04	1.0E+05	1.0E+05	7.1E-02	5.5E+02	7.5E+00	4.1E+01	2.4E+02	2.0E+00	6.7E+01	1.7E+00
7.0E+04	7.0E+05	4.9E+06	2.9E-01	f	f	4.3E+02	f	1.7E+03	f	3.1E+03
4.0E+05	7.0E+06	2.8E+08	1.2E+02	f	f	f	f	f	f	f
7.0E+05	7.0E+06	4.9E+08	3.2E+02	f	f	f	f	f	f	f
7.5E+05	7.5E+06	5.6E+08	4.7E+02	f	f	f	f	f	f	f
10 ⁻⁶										
1.0E+04	1.0E+05	1.0E+05	1.1E-01	1.1E+03	1.6E+01	4.3E+01	2.5E+02	3.6E+00	6.7E+01	2.1E+00
7.0E+04	7.0E+05	4.9E+06	8.4E-01	f	f	f	f	2.5E+03	f	3.5E+03
4.0E+05	7.0E+06	2.8E+08	2.6E+02	f	f	f	f	f	f	f
7.0E+05	7.0E+06	4.9E+08	5.2E+02	f	f	f	f	f	f	f
7.5E+05	7.5E+06	5.6E+08	6.0E+02	f	f	f	f	f	f	f

Note. Entries marked “f” indicate failure due to exceeding the time limit or returning errors. Bold entries indicate the best runtime among all solvers for each row. Shaded cells highlight the best-performing method on the original problem (without presolve).

It is observed from Table 6 that, for Lasso problems, cuPDCS consistently achieves the best performance among all tested solvers, including both first-order and interior-point methods, whether or not presolve is applied. To evaluate scalability, we examined instances with matrix dimensions $m = 7.5 \times 10^5$ and $n = 7.5 \times 10^5$. Even at this extreme scale, cuPDCS successfully computed high-accuracy solutions within a practical time frame. Moreover, cuPDCS shows only a modest increase in runtime when transitioning from a target tolerance of 10^{-3} to 10^{-6} . This near-constant runtime indicates that the underlying PDCS algorithm converges faster (potentially at a linear rate) on Lasso problems compared to Fisher market equilibrium problems. This conjecture is further supported by the empirical convergence behavior illustrated in Figure 6 in Section 5.5.

While presolve continues to benefit interior-point solvers like COPT and MOSEK, the improvement is less significant than in the Fisher market experiments. In contrast, GPU acceleration offers greater advantages. Specifically, CuClarabel demonstrates performance comparable to that of both COPT* and MOSEK*. However, its applicability is confined to moderate problem sizes, as it struggles to solve very large-scale instances and is slower than commercial solvers on small-scale instances.

5.4 Multi-period Portfolio Optimization Problems

The Fisher market problem we have tested in Section 5.2 contains a huge number of small cones, each with three dimensions. In contrast, the Lasso problem in this section, despite being high-dimensional and large-scale, contains only a single second-order cone. In this section, we test on the Multi-period Portfolio Optimization (MPO) problems that contain multiple different cones.

The Fisher market problems discussed in Section 5.2 involve a very large number of small cones, each with three dimensions. In contrast, the Lasso problems examined in the previous section, although high-dimensional and large-scale, contain only a single second-order cone. In this section, we study Multi-Period Portfolio Optimization (MPO) problems, which include a mix of multiple cone types and increasingly higher problem dimensions as the number of time periods grows.

A typical MPO problem is formulated as follows [9]:

$$\begin{aligned}
& \max_{\mathbf{w}_{\tau+1}, \tau=0, \dots, T-1} \sum_{\tau=0}^{T-1} \langle \hat{\mathbf{r}}_{\tau}, \mathbf{w}_{\tau+1} \rangle \\
& \text{s. t. } \mathbf{1}^{\top} (\mathbf{w}_{\tau+1} - \mathbf{w}_{\tau}) = 0, \quad \forall \tau = 0, \dots, T-1 \\
& \quad \mathbf{w}_{\tau} \geq 0, \quad \forall \tau = 0, \dots, T-1 \\
& \quad (\mathbf{w}_{\tau}^m)_{[n]} \hat{\Sigma}_{\tau+1} (\mathbf{w}_{\tau+1})_{[n]} = 0, \quad \forall \tau = 0, \dots, T-1 \\
& \quad \left\| \hat{\Sigma}_{\tau+1}^{1/2} (\mathbf{w}_{\tau+1} - \mathbf{w}_b)_{[n]} \right\| \leq \gamma_{1\tau}, \quad \forall \tau = 0, \dots, T-1 \\
& \quad -\gamma_{2\tau, i} \leq (\mathbf{w}_{\tau+1} - \mathbf{w}_{\tau})_i \leq \gamma_{2\tau, i}, \quad \forall \tau = 0, \dots, T-1, i = 1, \dots, n+1 \\
& \quad -\gamma_{3\tau} \leq \sum_{i=1}^n \left(\hat{\Sigma}_{\tau+1}^{1/2} \right)_{ii} (\mathbf{w}_{\tau+1} - \mathbf{w}_b)_i \leq \gamma_{3\tau}, \quad \forall \tau = 0, \dots, T-1.
\end{aligned}$$

In the above optimization problem, $\hat{\mathbf{r}}_{\tau}$ represents the estimated future return at time τ , \mathbf{w}_{τ} denotes the investment weight of the portfolio at time τ , $\hat{\Sigma}_{\tau}$ is the estimated variance of future returns at time τ , \mathbf{w}_b is the benchmark portfolio (set as an all-cash strategy), and $\hat{\mathbf{w}}_{\tau}^m$ represents the estimated price of securities at time τ . Within this framework, the objective is to maximize the multi-period return. The first equality constraint ensures that the sum of transaction weights is zero, while the second inequality, $\mathbf{w}_{\tau} \geq 0$, enforces long-only holdings. The third equality imposes a market-neutral condition, and the fourth inequality serves as a risk control mechanism. The fifth inequality restricts the transaction weight of a single period to a specified range, and the final inequality controls the estimation error for $\hat{\Sigma}$. Further details and explanations can be found in [9].

We select all securities from five major indices—S&P 500, NASDAQ-100, DOW 30, FTSE 100, and Nikkei 225—resulting in 844 assets in total. The historical data used to construct the problem was retrieved using the `cvxportfolio` package [9], which sources prices from Yahoo Finance. Data from the year 2024 is used to estimate the returns, variances, and prices for the first period. For subsequent periods, the predicted data was generated by introducing a controlled level of random noise to the first period's estimates. The parameters are set as follows: $\gamma_{1\tau} = \left\| \hat{\Sigma}_{\tau+1}^{1/2} (\mathbf{w}_{1/n} - \mathbf{w}_b) \right\|$, $\gamma_{2\tau, i} = 0.05$, and $\gamma_{3\tau} = 0.05$, where $\mathbf{w}_{1/n}$ denotes the equally weighted $1/n$ strategy.

We still evaluate solver performance on MPO problems under two levels of solution accuracy: low accuracy (10^{-3}) and high accuracy (10^{-6}). Results are presented in Table 7. As the number of time periods T increases, the number of constraints, variables, and cones grows proportionally.

From Table 7, we observe that cuPDCS consistently outperforms the other first-order solvers, SCS(indirect) and ABIP. Notably, ABIP is available only as a CPU implementation and still relies

Table 7: Experiments on MPO problems.

T	Without Presolve						With Presolve	
	cuPDCS	SCS(GPU)	ABIP	CuClarabel	COPT	MOSEK	COPT*	MOSEK*
10^{-3}								
3	1.9E+00	3.7E+00	1.9E+00	1.5E+00	8.3E-01	8.1E-01	8.6E-01	4.0E-02
48	7.2E+00	3.5E+02	4.0E+01	9.9E+01	8.8E+00	1.7E+01	9.3E+00	8.6E-01
96	1.1E+01	1.8E+03	9.1E+01	6.3E+02	1.9E+01	3.3E+01	2.0E+01	1.7E+00
360	5.1E+01	f	1.9E+02	f	1.2E+02	1.2E+02	1.2E+02	7.2E+00
1440	4.9E+02	f	9.0E+02	f	f	f	f	4.8E+01
2160	5.8E+02	f	f	f	f	f	f	f
3600	1.1E+03	f	f	f	f	f	f	f
10^{-6}								
3	7.5E+00	f	f	1.6E+00	8.3E-01	1.3E+00	8.4E-01	5.0E-02
48	1.8E+01	f	f	1.1E+02	8.8E+00	2.7E+01	8.8E+00	9.9E-01
96	5.7E+01	f	f	6.1E+02	1.9E+01	6.0E+01	1.9E+01	1.9E+00
360	4.2E+02	f	f	9.2E+03	1.2E+02	2.4E+02	1.1E+02	8.2E+00
1440	3.4E+03	f	f	f	f	f	f	5.6E+01
2160	1.0E+03	f	f	f	f	f	f	f
3600	9.0E+03	f	f	f	f	f	f	f

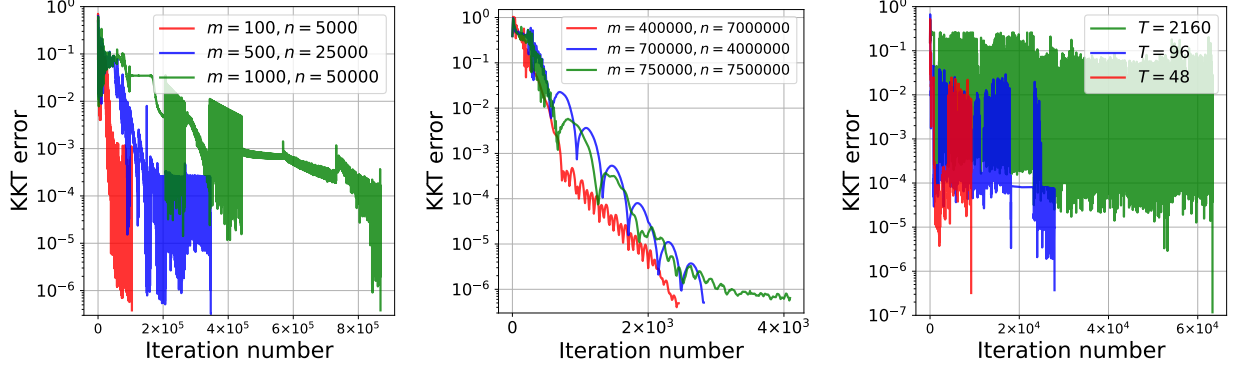
Note. Entries marked “f” indicate failure due to exceeding the time limit or returning errors. Bold entries indicate the best runtime among all solvers for each row. Shaded cells highlight the best-performing method on the original problem (without presolve).

on at least one matrix factorization per iteration, making it less suitable for large-scale problems. Among the solvers that work directly on the original problem formulation (i.e., without presolve), cuPDCS demonstrates a clear advantage on large-scale instances.

However, as the desired accuracy increases, the runtime of cuPDCS grows more rapidly than that of interior-point methods. Presolve can significantly enhance MOSEK’s performance, making it indeed more robust and quicker on moderate-sized instances. Yet, even MOSEK* struggles to handle large-scale MPO problems due to its considerable memory requirements. For cases with $T \geq 2160$, MOSEK* runs out of memory, whereas cuPDCS continues to perform effectively. These results show the scalability and robustness of cuPDCS for solving large-scale conic optimization problems involving mixed cone types.

5.5 Comments and Remarks

To provide further insight into the algorithmic behavior of PDCS, we illustrate its convergence on several representative problem instances in Figure 6. Each plot shows the evolution of the “KKT error” across iterations of PDCS. Here, the “KKT error” is defined as the average of the three error metrics introduced in (21). Figures 6a and 6c illustrate the convergence behavior for three Fisher market equilibrium problems and three MPO problems, respectively. In both cases, we observe an initial phase of rapid progress followed by a plateau with slower KKT error reduction. This trend helps explain why PDCS is particularly effective in computing low-accuracy solutions.



(a) Fisher market equilibrium problem (Section 5.2) (b) LASSO problem (Section 5.3) (c) MPO problem (Section 5.4)

Figure 6: Convergence behavior of PDCS.

Interestingly, during the final iterations, PDCS often exhibits a phase of accelerated convergence, which differs from the typical sublinear behavior expected from first-order methods. Figure 6b shows the convergence of PDCS on three Lasso problem instances. In this case, the algorithm exhibits nearly linear convergence, enabling it to achieve high-accuracy solutions in a relatively short time. This observation is consistent with the results reported in Section 5.3 and suggests Lasso problem is particularly well-suited for the rPDHG. It would be interesting to explore what properties of conic problems (such as Lasso problems) could make them particularly suitable for PDCS.

In summary, cuPDCS demonstrates consistently strong performance across a wide range of large-scale conic optimization problems. It outperforms other first-order methods, such as SCS and ABIP, particularly in high-dimensional problems by GPU enhancements. Moreover, even in comparison with commercial interior-point solvers like MOSEK and COPT (both with and without presolve), cuPDCS remains highly competitive. Its advantages are especially pronounced in large-scale, lower-accuracy settings. It would be interesting to study the presolve for first-order methods like cuPDCS, as it could potentially lead to another significant speedup, similar to the presolve for MOSEK.

Acknowledgement

Z. Xiong was supported by AFOSR Grant No. FA9550-22-1-0356. The authors thank Haihao Lu for sharing their progress on developing a large-scale SOCP solver during the final preparation of this manuscript.

Appendices

A How to compute the normalized duality gap?

The main idea of computing the normalized duality gap is similar to that developed in [2] for LPs and [63] for CLPs. Below, we restate it in the context of our CLP formulation (P).

Note that

$$\rho^{\mathbf{N}}(r; \mathbf{z}) := \frac{1}{r} \cdot \left(\begin{array}{ll} \max_{\hat{\mathbf{z}}} & \mathbf{b}^\top (\hat{\mathbf{z}} - \mathbf{z}) \\ \text{s. t.} & \hat{\mathbf{z}} \in \mathcal{X} \times \mathcal{Y}, \|\mathbf{z} - \hat{\mathbf{z}}\|_{\mathbf{N}}^2 \leq r^2 \end{array} \right) \quad (23)$$

where $\mathbf{b} = \begin{pmatrix} \mathbf{b}_1 \\ \mathbf{b}_2 \end{pmatrix} = \begin{pmatrix} \mathbf{G}^\top \mathbf{y} - \mathbf{c} \\ \mathbf{h} - \mathbf{G}\mathbf{x} \end{pmatrix}$. As shown in [2, 63], the optimal solution of (23) coincides with the solution $\mathbf{z}(t)$ of the following problem such that $\|\mathbf{z} - \mathbf{z}(t)\| = r$:

$$\mathbf{z}(t) := \operatorname{argmax}_{\tilde{\mathbf{z}} \in \mathcal{X} \times \mathcal{Y}} \quad t \cdot \mathbf{b}^\top (\tilde{\mathbf{z}} - \mathbf{z}) - \frac{1}{2} \cdot \|\tilde{\mathbf{z}} - \mathbf{z}\|_{\mathbf{N}}^2. \quad (24)$$

Therefore, the goal becomes finding the t such that $\|\mathbf{z} - \mathbf{z}(t)\|_{\mathbf{N}} = r$ and we use t_p to denote this t . We use a binary search method to identify the t_p and compute $\rho^{\mathbf{N}}(r; \mathbf{z})$. See the overall algorithm of computing such t_p within a tolerance ε and the corresponding $\rho^{\mathbf{N}}(r; \mathbf{z})$ in Algorithm 4.

Algorithm 4 Binary search for normalized duality gap $\rho(r; \mathbf{z})$

Require: $t_0, \mathbf{z} = (\mathbf{x}, \mathbf{y}), r$

```

1:  $t_{\text{left}} = 0, t_{\text{right}} = t_0$ 
2: for  $k = 0, 1, \dots$ , do  $\triangleright$  Find an initial interval  $[t_{\text{left}}, t_{\text{right}}]$  by exponential search
3:    $\tilde{\mathbf{z}} \leftarrow \mathbf{z}(t_k)$ 
4:   if  $\|\mathbf{z} - \tilde{\mathbf{z}}\|_{\mathbf{N}} > r$  then
5:     if  $k = 0$  then
6:       | quit the loop
7:     else
8:       |  $t_{\text{right}} \leftarrow t_k, t_{\text{left}} \leftarrow t_k/2$ , and quit the loop
9:    $t_{k+1} \leftarrow 2t_k$ 
10: while  $t_{\text{right}} - t_{\text{left}} > \varepsilon$  do  $\triangleright$  Refine  $[t_{\text{left}}, t_{\text{right}}]$  by binary search
11:    $t_{\text{mid}} \leftarrow (t_{\text{left}} + t_{\text{right}})/2$ 
12:    $\tilde{\mathbf{z}} \leftarrow \mathbf{z}(t_{\text{mid}})$ 
13:   if  $\|\mathbf{z} - \tilde{\mathbf{z}}\|_{\mathbf{N}} < r$  then
14:     |  $t_{\text{left}} \leftarrow t_{\text{mid}}$ 
15:   else
16:     |  $t_{\text{right}} \leftarrow t_{\text{mid}}$ 
17: return  $\frac{\mathbf{b}^\top (\tilde{\mathbf{z}} - \mathbf{z})}{r}$ 

```

The problem (24) is essentially a Euclidean projection onto the feasible set $\mathcal{X} \times \mathcal{Y}$:

$$\mathbf{z}(t) = (\operatorname{Proj}_{\mathcal{X}}(\mathbf{x} + t\tau \cdot \mathbf{b}_1), \operatorname{Proj}_{\mathcal{Y}}\{\mathbf{y} + t\sigma \cdot \mathbf{b}_2\}) , \quad (25)$$

which reduces to multiple cone projection problems because $\mathcal{X} = [\mathbf{l}, \mathbf{u}] \times \mathcal{K}_p$ and $\mathcal{Y} = \mathcal{K}_d$. Appendix B will show more details on how to do these cone projections efficiently.

B Projection onto a rescaled exponential cone

In this section, we will provide a detailed discussion of how to project onto an exponential cone, with a particular focus on the case of diagonal rescaling.

The following theorem shows that the solution pair \mathbf{v}_p and \mathbf{v}_d from (20) can be parameterized by a scalar ρ , which can be obtained by solving a root-finding problem.

Theorem 2. *The projection of $\mathbf{v}_0 = (r_0, s_0, t_0) \in \mathbb{R}^3$ onto the rescaled cone $\mathbf{D}\mathcal{K}_{\text{exp}}$ is given as follows:*

1. If $\mathbf{v}_0 \in \mathbf{D}\mathcal{K}_{\text{exp}}$, then $\text{Proj}_{\mathbf{D}\mathcal{K}_{\text{exp}}}(\mathbf{v}_0) = \mathbf{v}_0$.
2. If $\mathbf{v}_0 \in -\mathbf{D}^{-1}\mathcal{K}_{\text{exp}}^*$, then $\text{Proj}_{\mathbf{D}\mathcal{K}_{\text{exp}}}(\mathbf{v}_0) = \mathbf{0}_{3 \times 1}$.
3. If $r_0 \leq 0$ and $s_0 \leq 0$, then $\mathbf{v}_p = (r_0, 0, t_0^+)$ and $\mathbf{v}_d = (0, s_0, t_0^-)$.
4. Otherwise, let $\rho \in \mathbb{R}$ be a scalar parameter satisfying the following system:

$$d_t \exp(\rho) s_p - d_t^{-1} \exp(-\rho) r_d - t_0 = 0, \quad s_p > 0, \quad r_d > 0 \quad (26)$$

in which

$$\mathbf{v}_p = (d_r \rho, d_s, d_t \exp(\rho)) s_p, \quad \text{with} \quad s_p = \frac{s_0 d_r^{-1} d_s - r_0 (1 - \rho)}{d_s^2 d_r^{-1} + d_r \rho (\rho - 1)}, \quad (27)$$

$$\mathbf{v}_d = (d_r^{-1}, (1 - \rho) d_s^{-1}, -d_t^{-1} \exp(-\rho)) r_d, \quad \text{with} \quad r_d = \frac{d_s^2 r_0 - d_s d_r \rho s_0}{d_s^2 d_r^{-1} + d_r \rho (\rho - 1)}. \quad (28)$$

Then \mathbf{v}_p and \mathbf{v}_d are the projections of \mathbf{v}_0 onto $\mathbf{D}\mathcal{K}_{\text{exp}}$ and $-\mathbf{D}^{-1}\mathcal{K}_{\text{exp}}^*$, respectively; i.e., $\mathbf{v}_d = \text{Proj}_{\mathbf{D}\mathcal{K}_{\text{exp}}}(\mathbf{v}_0)$ and $\mathbf{v}_d = \text{Proj}_{-\mathbf{D}^{-1}\mathcal{K}_{\text{exp}}^*}(\mathbf{v}_0)$.

In the practical implementation of PDCS, the system (26) is solved by a bijection method.

Theorem 2 provides the solution of (20). The first three cases of Theorem 2 are some simple cases, which are essentially the cases satisfying the elementwise orthogonality condition. In practice, we first check the first three cases, followed by solving the root-finding problem of the nonlinear system (26). Our strategy is built upon the projection algorithm for the unscaled exponential cone [22], yet the diagonal scaling matrix introduces a non-trivial coupling that complicates the root-finding analysis.

C Conic program reformulation

C.1 Fisher market equilibrium problem

In this section, we give the conic program reformulation of the Fisher market equilibrium problem (Section 5.2). The Fisher market equilibrium problem is equivalently written as the following

problem:

$$\begin{aligned}
& \min_{\mathbf{p} \in \mathbb{R}^m, \mathbf{X} \in \mathbb{R}^{m \times n}, \mathbf{t} \in \mathbb{R}^m} - \sum_{i \in [m]} \mathbf{w}_i \mathbf{p}_i, \\
& \text{s. t.} \quad \sum_{i \in [m]} \mathbf{X}_{ij} = \mathbf{b}_j, \quad \forall j \in [n], \\
& \quad \mathbf{t}_i = \sum_{j \in [n]} \mathbf{U}_{ij} \mathbf{X}_{ij}, \quad \forall i \in [m], \\
& \quad \mathbf{p}_i \leq \log(\mathbf{t}_i), \quad \forall i \in [m], \\
& \quad \mathbf{X}_{ij} \geq 0, \quad \forall i \in [m], j \in [n],
\end{aligned} \tag{29}$$

where $\mathbf{w} \in \mathbb{R}^m, \mathbf{U} \in \mathbb{R}^{m \times n}$ are given beforehand as the vector of monetary endowment for each buyer and the matrix of the utility vector for each buyer.

Now we present the conic program formulation of the problem. Let the decision variables be stacked as $\mathbf{y} \in \mathbb{R}^{m(n+2)}$:

$$\mathbf{y} = \left[\mathbf{X}_{:,1}^\top, \dots, \mathbf{X}_{:,n}^\top, (\mathbf{p}_1, \mathbf{t}_1), \dots, (\mathbf{p}_m, \mathbf{t}_m) \right]^\top.$$

Let the problem parameters be stacked as follows in $\mathbf{c}, \mathbf{A}, \tilde{\mathbf{b}}, \mathbf{Q}, \mathbf{d}$:

$$\begin{aligned}
\mathbf{c} &:= \left[\underbrace{0, \dots, 0}_{mn \text{ items}}, (-\mathbf{w}_1, 0), \dots, (-\mathbf{w}_m, 0) \right]^\top, \\
\mathbf{A} &:= \begin{bmatrix} \mathbf{I}_{n \times n} & \cdots & \mathbf{I}_{n \times n} & & \\ \mathbf{U}_{1,:} & & & (0, -1) & \\ & \cdots & & \cdots & \\ & & \mathbf{U}_{m,:} & & (0, -1) \end{bmatrix}, \quad \tilde{\mathbf{b}} := \begin{bmatrix} \mathbf{b} \\ \mathbf{0}_{m \times 1} \end{bmatrix} \\
\mathbf{Q} &:= \begin{bmatrix} \mathbf{0}_{3 \times 1} & \begin{pmatrix} 1 & & \\ & & 1 \end{pmatrix} & & \\ & & \cdots & \\ & & & \begin{pmatrix} 1 & & \\ & & 1 \end{pmatrix} \end{bmatrix}, \quad \mathbf{d} := \begin{bmatrix} \begin{pmatrix} 0 \\ -1 \\ 0 \end{pmatrix} \\ \cdots \\ \begin{pmatrix} 0 \\ -1 \\ 0 \end{pmatrix} \end{bmatrix}.
\end{aligned}$$

Then (29) is equivalent to the following conic program problem:

$$\min_{\mathbf{y} \in \mathbb{R}^{m(n+2)}} \mathbf{c}^\top \mathbf{y}, \quad \text{s. t. } \mathbf{A}\mathbf{y} = \tilde{\mathbf{b}}, \quad \mathbf{Q}\mathbf{y} - \mathbf{d} \in \mathcal{K}_{\text{exp}}^m, \quad \mathbf{y} \geq \mathbf{1} \tag{30}$$

where $\mathcal{K}_{\text{exp}}^m := \underbrace{\mathcal{K}_{\text{exp}} \times \cdots \times \mathcal{K}_{\text{exp}}}_{m \text{ items}}$ and $\mathbf{l} := [\underbrace{0, \dots, 0}_{mn \text{ items}}, \underbrace{-\infty, \dots, -\infty}_{2m \text{ items}}]$.

The above problem (30) is the problem that the various solvers, including cuPDCS, directly address in the experiments in Section 5.2.

C.2 Lasso Problem

For completeness, we present the SOCP reformulation of the Lasso problem. The original Lasso problem is formulated as

$$\min_{\mathbf{x} \in \mathbb{R}^n} \|\mathbf{A}\mathbf{x} - \mathbf{b}\|^2 + \lambda \|\mathbf{x}\|_1,$$

where $\mathbf{A} \in \mathbb{R}^{m \times n}$. Its SOCP reformulation is given by

$$\begin{aligned} \min_{\substack{w \in \mathbb{R}, r \in \mathbb{R}, \mathbf{y} \in \mathbb{R}^m \\ \mathbf{x}_1 \in \mathbb{R}_+^n, \mathbf{x}_2 \in \mathbb{R}_+^n}} \quad & \left\langle \begin{bmatrix} 0 & 2 & (\mathbf{0}_{m \times 1})^\top & \lambda \cdot (\mathbf{1}_{2n \times 1})^\top \end{bmatrix}^\top, \begin{bmatrix} w & r & \mathbf{y}^\top & \mathbf{x}_1^\top & \mathbf{x}_2^\top \end{bmatrix}^\top \right\rangle \\ \text{s. t.} \quad & \begin{bmatrix} 1 & 0 & 0 & \cdots & 0 \\ \mathbf{0}_{m \times 1} & \mathbf{0}_{m \times 1} & \mathbf{I}_{m \times m} & \mathbf{A} & -\mathbf{A} \end{bmatrix} \begin{bmatrix} w & r & \mathbf{y}^\top & \mathbf{x}_1^\top & \mathbf{x}_2^\top \end{bmatrix}^\top = \begin{bmatrix} 1 \\ \mathbf{b} \end{bmatrix} \\ & \begin{bmatrix} \frac{w+r}{2} & \frac{w-r}{2} & \mathbf{y}^\top \end{bmatrix}^\top \in \mathcal{K}_{\text{soc}}^{m+2} \end{aligned}$$

C.3 Multi-period Portfolio Optimization (MPO)

In this subsection, we present the MPO problem and its conic program reformulation. Compared with single-period portfolio optimization problems, MPO can avoid creating a greedy strategy and amortize the transaction in multi periods.

Boyd et al. [9] present a penalty-based formulation of the Multi-Period Optimization (MPO) problem, as given below in equation (31):

$$\begin{aligned} \max_{\substack{\mathbf{w}_{\tau+1}, \mathbf{z}_\tau \in \mathbb{R}^{n+1}: \\ \tau=0, \dots, T-1}} \quad & \sum_{\tau=0}^{T-1} \left\{ \hat{\mathbf{r}}_{\tau+1}^\top \mathbf{w}_{\tau+1} - \gamma_\tau^{\text{risk}} \hat{\psi}_\tau(\mathbf{w}_{\tau+1}) - \gamma_\tau^{\text{hold}} \hat{\phi}_\tau^{\text{hold}}(\mathbf{w}_{\tau+1}) - \gamma_\tau^{\text{trade}} \hat{\phi}_\tau^{\text{trade}}(\mathbf{z}_\tau) \right\} \\ \text{s. t.} \quad & \mathbf{1}^\top \mathbf{z}_\tau = 0, \quad \mathbf{z}_\tau \in \mathcal{Z}_\tau, \quad \mathbf{w}_\tau + \mathbf{z}_\tau \in \mathcal{W}_\tau, \quad \text{for all } \tau = 0, \dots, T-1, \\ & \mathbf{w}_{\tau+1} = \mathbf{w}_\tau + \mathbf{z}_\tau, \quad \text{for all } \tau = 0, \dots, T-1, \end{aligned} \tag{31}$$

where the decision variable $\mathbf{w}_{\tau+1} \in \mathbb{R}^{n+1}$ represents the weights of assets for the period $\tau + 1$, in which the first n components denote n assets and the $(n + 1)$ -th component denotes the weight of cash. And the other decision variable \mathbf{z}_τ denotes the transaction amount in the period τ .

In this formulation, the expected return $\hat{\mathbf{r}}_{\tau+1} \in \mathbb{R}^{n+1}$ is predicted beforehand using other statistical or machine learning methods. The function $\hat{\psi}_\tau(\cdot)$ quantifies risk, which is typically defined as $\hat{\psi}_\tau(\mathbf{w}_{\tau+1}) := \|\hat{\Sigma}_{\tau+1}^{1/2}[\mathbf{w}_{\tau+1} - \mathbf{w}_b]_{[n]}\|^2 + \kappa(\sum_{i=1}^n \hat{\Sigma}_{ii}^{1/2} |\mathbf{w}_{\tau+1} - \mathbf{w}_b|_{(i)})^2$. In this formulation, \mathbf{w}_b denotes the benchmark asset weight and $\hat{\Sigma}$ is an estimate of the covariance matrix of the stochastic returns,

and the term $(\sum_{i=1}^n \hat{\Sigma}_{ii}^{1/2} |\mathbf{w}_{\tau+1} - \mathbf{w}_b|_{(i)})^2$ is a measure of covariance forecast error risk and κ is a hyper-parameter [33, 36]. The term $\hat{\phi}_\tau^{\text{hold}}$ denotes the holding cost, which may include factors such as borrowing fees. The term $\hat{\phi}_\tau^{\text{trade}}(\mathbf{z}_\tau)$ denotes the transaction cost, which is typically modeled as a linear and quadratic function of the transaction amount \mathbf{z}_τ , i.e., $\hat{\phi}_\tau^{\text{trade}}([\mathbf{z}_\tau]_i) = a_{\tau,i} |[\mathbf{z}_\tau]_i| + b_{\tau,i} |[\mathbf{z}_\tau]_{(i)}|^2$ where a_τ and b_τ are coefficients [27] that can be predicted using other statistical and machine learning methods. The set \mathcal{Z}_τ contains the constraints for the transaction amounts \mathbf{z}_τ , such as limiting the transaction ratio in each period. The set \mathcal{W}_τ contains the constraints on the asset weights $\mathbf{w}_{\tau+1}$, such as the requirement for market neutrality, $(\mathbf{w}_\tau^m)^\top \hat{\Sigma}_\tau(\mathbf{w}_{\tau+1}) = 0$ where \mathbf{w}_τ^m is the asset value in period τ .

Hence, a specific example of (31) is

$$\begin{aligned}
& \max_{\substack{\mathbf{w}_{\tau+1} \in \mathbb{R}^{n+1}: \\ \tau=0, \dots, T-1}} \sum_{\tau=0}^{T-1} \left[\hat{\mathbf{r}}_{\tau+1}^\top \mathbf{w}_{\tau+1} - \underbrace{\gamma_\tau^{\text{risk}} \left(\left\| \hat{\Sigma}_{\tau+1}^{1/2} [\mathbf{w}_{\tau+1} - \mathbf{w}_b]_{[n]} \right\|^2 + \kappa \left(\sum_{i=1}^n \hat{\Sigma}_{\tau+1,ii}^{1/2} |[\mathbf{w}_{\tau+1} - \mathbf{w}_b]_i| \right)^2 \right)}_{\hat{\psi}_\tau^{\text{risk}}(\mathbf{w}_{\tau+1})} \right. \\
& \quad \left. - \underbrace{\gamma_\tau^{\text{trade}} \cdot \left(\sum_{i=1}^n a_{\tau,i} |\mathbf{w}_{\tau+1} - \mathbf{w}_\tau|_i - b_{\tau,i} (\mathbf{w}_{\tau+1} - \mathbf{w}_\tau)_i^2 \right)}_{\hat{\phi}_\tau^{\text{trade}}(\mathbf{w}_{\tau+1})} - \gamma_\tau^{\text{hold}} \cdot \underbrace{0}_{\hat{\phi}_\tau^{\text{hold}}(\mathbf{w}_{\tau+1})} \right] \\
& \text{s. t.} \quad \mathbf{1}^\top (\mathbf{w}_{\tau+1} - \mathbf{w}_\tau) = 0, \quad \mathbf{w}_{\tau+1} \geq 0, \quad (\mathbf{w}_\tau^m)_{[n]}^\top \hat{\Sigma}_\tau(\mathbf{w}_{\tau+1})_{[n]} = 0, \quad \tau = 0, \dots, T-1.
\end{aligned} \tag{32}$$

This specific example considers the case with no borrowing fee, long holding, and no constraint on transactions. In this formulation, $\gamma_\tau^{\text{risk}}, \kappa, \gamma_\tau^{\text{trade}}, a_{\tau,i}, b_{\tau,i}, \gamma_\tau^{\text{hold}}$ are hyper-parameters.

The above problem models the risk-control tasks in the portfolio optimization problem as regularization terms added to the objective function, but choosing the proper hyperparameters to balance different objectives would be difficult in practice and require heavy parameter tuning. Given that, another commonly seen strategy is to model the other objectives other than profit within the constraints. In this way, the hyper-parameters directly correspond to the maximum allowed holding costs, transaction cost, or risk. See, for example, [35]. Such a constraint-based formulation of (32) is as follows, a SOCP problem:

$$\begin{aligned}
& \max_{\substack{\mathbf{w}_{\tau+1} \in \mathbb{R}^{n+1}; \\ \tau=0, \dots, T-1}} \sum_{\tau=0}^{T-1} \hat{\mathbf{r}}_{\tau}^{\top} \mathbf{w}_{\tau+1} \\
& \text{s. t.} \quad \mathbf{1}^{\top} (\mathbf{w}_{\tau+1} - \mathbf{w}_{\tau}) = 0, \quad \forall \tau = 0, \dots, T-1 \\
& \quad \mathbf{w}_{\tau} \geq 0, \quad \forall \tau = 0, \dots, T-1 \\
& \quad (\mathbf{w}_{\tau}^m)_{[n]} \hat{\Sigma}_{\tau+1} (\mathbf{w}_{\tau+1})_{[n]} = 0, \quad \forall \tau = 0, \dots, T-1 \\
& \quad \left\| \hat{\Sigma}_{\tau+1}^{1/2} (\mathbf{w}_{\tau+1} - \mathbf{w}_b)_{[n]} \right\| \leq \gamma_{1\tau}, \quad \forall \tau = 0, \dots, T-1 \\
& \quad -\gamma_{2\tau, i} \leq (\mathbf{w}_{\tau+1} - \mathbf{w}_{\tau})_i \leq \gamma_{2\tau, i}, \quad \forall \tau = 0, \dots, T-1, i = 1, \dots, n+1 \\
& \quad -\gamma_{3\tau} \leq \sum_{i=1}^n \left(\hat{\Sigma}_{\tau+1}^{1/2} \right)_{ii} (\mathbf{w}_{\tau+1} - \mathbf{w}_b)_i \leq \gamma_{3\tau}, \quad \forall \tau = 0, \dots, T-1.
\end{aligned} \tag{33}$$

The above problem (33) is the problem that the various solvers, including cuPDCS, directly address in the experiments in Section 5.4.

D Optimality Termination Criteria

This section describes the termination criteria of the solvers used in our experiments on CLP problems. Generally, these criteria comprise three types of different errors: primal infeasibility (err_p), dual infeasibility (err_d), and the duality gap (err_{gap}).

D.1 ABIP

ABIP directly addresses the following primal and dual problems:

$$\begin{aligned}
& \min_{\mathbf{x}} \quad \mathbf{c}^{\top} \mathbf{x} \quad \text{s. t.} \quad \mathbf{A} \mathbf{x} = \mathbf{b}, \quad \mathbf{x} \in \mathcal{K}, \\
& \max_{\mathbf{y}} \quad \mathbf{b}^{\top} \mathbf{y} \quad \text{s. t.} \quad \mathbf{A}^{\top} \mathbf{y} + \mathbf{s} = \mathbf{c}, \quad \mathbf{s} \in \mathcal{K}^*.
\end{aligned} \tag{34}$$

If the given optimization problem does not satisfy this formulation, ABIP reformulates the problem to (34) first and then solves it. It should be noted that for all iterates of ABIP, \mathbf{x} and \mathbf{s} always lie in the cones \mathcal{K} and \mathcal{K}^* because ABIP uses an ADMM-based interior point method, which ensures all iterates are always in the interior of the cones. On the formulation (34), ABIP determines its termination criteria based on the following three types of errors:

$$\text{err}_p := \frac{\|\mathbf{A} \mathbf{x} - \mathbf{b}\|_{\infty}}{1 + \max\{\|\mathbf{A} \mathbf{x}\|_{\infty}, \|\mathbf{b}\|_{\infty}\}}, \quad \text{err}_d := \frac{\|\mathbf{c} - \mathbf{A}^{\top} \mathbf{y} - \mathbf{s}\|_{\infty}}{1 + \|\mathbf{c}\|_{\infty}}, \quad \text{err}_{\text{gap}} := \frac{|\mathbf{c}^{\top} \mathbf{x} + \mathbf{b}^{\top} \mathbf{y}|}{1 + \max\{|\mathbf{c}^{\top} \mathbf{x}|, |\mathbf{b}^{\top} \mathbf{y}|\}}.$$

In our experiments, we say a solution satisfies the ε_{rel} tolerance if $\max\{\text{err}_p, \text{err}_d, \text{err}_{\text{gap}}\} \leq \varepsilon_{\text{rel}}$ for this solution.

D.2 SCS

SCS directly solves the conic program problems in the following formulation:

$$\begin{aligned} \min_{\mathbf{x}} \quad & \mathbf{c}^\top \mathbf{x} \quad \text{s.t. } \mathbf{Ax} + \mathbf{s} = \mathbf{b}, \quad \mathbf{s} \in \mathcal{K}, \\ \max_{\mathbf{y}} \quad & -\mathbf{b}^\top \mathbf{y} \quad \text{s.t. } \mathbf{A}^\top \mathbf{y} + \mathbf{c} = 0, \quad \mathbf{y} \in \mathcal{K}^*. \end{aligned} \quad (35)$$

If the problem is not in this formulation, we should first reformulate it into this formulation and then use SCS to solve it. All iterates of SCS satisfy the conic constraints $\mathbf{s} \in \mathcal{K}$ and $\mathbf{y} \in \mathcal{K}^*$ as the solver does projections onto the cones in each iteration.

On the formulation (35), SCS determines its termination criteria based on the following residual thresholds:

$$\begin{aligned} \text{err}_p &= \|\mathbf{Ax} + \mathbf{s} - \mathbf{b}\|_\infty \leq \varepsilon_{\text{abs}} + \varepsilon_{\text{rel}} \cdot \max \{\|\mathbf{Ax}\|_\infty, \|\mathbf{s}\|_\infty, \|\mathbf{b}\|_\infty\}, \\ \text{err}_d &= \|\mathbf{A}^\top \mathbf{y} + \mathbf{c}\|_\infty \leq \varepsilon_{\text{abs}} + \varepsilon_{\text{rel}} \cdot \max \left\{ \left\| \mathbf{A}^\top \mathbf{y} \right\|_\infty, \|\mathbf{c}\|_\infty \right\}, \\ \text{err}_{\text{gap}} &= |\mathbf{c}^\top \mathbf{x} - \mathbf{b}^\top \mathbf{y}| \leq \varepsilon_{\text{abs}} + \varepsilon_{\text{rel}} \cdot \max \left\{ |\mathbf{c}^\top \mathbf{x}|, |\mathbf{b}^\top \mathbf{y}| \right\}. \end{aligned}$$

In our experiments, we say a solution satisfies the ε tolerance if the above conditions all hold with $\varepsilon_{\text{rel}} = \varepsilon_{\text{abs}} = \varepsilon$.

D.3 COPT

The algorithm used in the solver COPT is an interior point method, but the definition of tolerance in its optimality criteria is not publicly available yet.

D.4 MOSEK

MOSEK uses an interior-point method to solve the conic program problem that is similarly structured to (34). However, it directly addresses the self-dual homogeneous model below:

$$\begin{aligned} \mathbf{Ax} - \mathbf{b}\tau &= 0 \\ \mathbf{A}^\top \mathbf{y} + \mathbf{s} - \mathbf{c}\tau &= 0 \\ -\mathbf{c}^\top \mathbf{x} + \mathbf{b}^\top \mathbf{y} - \kappa &= 0 \\ \mathbf{x} \in \mathcal{K}, \quad \mathbf{s} \in \mathcal{K}^*, \quad \tau, \kappa &\geq 0. \end{aligned}$$

A solution is regarded as satisfying the ε_{rel} tolerance in MOSEK if the following conditions hold:

$$\begin{aligned} \text{err}_p &= \frac{\|\mathbf{A}\frac{\mathbf{x}}{\tau} - \mathbf{b}\|_\infty}{1 + \|\mathbf{b}\|_\infty} \leq \varepsilon_{\text{rel}}, \\ \text{err}_d &= \frac{\|A^\top \frac{\mathbf{y}}{\tau} + \frac{\mathbf{s}}{\tau} - \mathbf{c}\|_\infty}{1 + \|\mathbf{c}\|_\infty} \leq \varepsilon_{\text{rel}}, \\ \text{err}_{\text{gap}} &= \max \left\{ \frac{x^\top \mathbf{s}}{\tau^2}, \left| \frac{\mathbf{c}^\top \mathbf{x}}{\tau} - \frac{\mathbf{b}^\top \mathbf{y}}{\tau} \right| \right\} / \max \left\{ 1, \frac{\min \{|\mathbf{c}^\top \mathbf{x}|, |\mathbf{b}^\top \mathbf{y}|\}}{\tau} \right\} \leq \varepsilon_{\text{rel}}. \end{aligned}$$

D.5 CuClarabel

The problem formulation that CuClarabel solves is similar to that of SCS, i.e., (35). However, CuClarabel introduces two slack variables $\tau, \kappa \geq 0$ and consider the following optimization problem:

$$\begin{aligned} \min \quad & \mathbf{s}^\top \mathbf{y} + \tau \kappa \\ \text{s. t.} \quad & \mathbf{c}^\top \mathbf{x} + \mathbf{b}^\top \mathbf{y} = -\kappa \\ & \mathbf{A}^\top \mathbf{y} + \mathbf{c}\tau = 0 \\ & \mathbf{A}\mathbf{x} + \mathbf{s} - \mathbf{b}\tau = 0 \\ & (\mathbf{s}, \mathbf{y}, \tau, \kappa) \in \mathcal{K} \times \mathcal{K}^* \times \mathbb{R}_+ \times \mathbb{R}_+. \end{aligned}$$

For the above formulation, a solution is regarded as satisfying the ε_{rel} tolerance if the following conditions hold:

$$\begin{aligned} \text{err}_p &= \frac{\|\mathbf{A}\frac{\mathbf{x}}{\tau} - \frac{\mathbf{s}}{\tau} + \mathbf{b}\|_\infty}{\max\{1, \|\mathbf{b}\|_\infty + \|\mathbf{x}/\tau\|_\infty + \|\mathbf{s}/\tau\|_\infty\}} \leq \varepsilon_{\text{rel}} \\ \text{err}_d &= \frac{\|\mathbf{A}^\top \frac{\mathbf{y}}{\tau} + \mathbf{c}\|_\infty}{\max\{1, \|\mathbf{c}\|_\infty + \|\mathbf{x}/\tau\|_\infty + \|\mathbf{z}/\tau\|_\infty\}} \leq \varepsilon_{\text{rel}} \\ \text{err}_{\text{gap}} &= \frac{|\mathbf{c}^\top \mathbf{x} + \mathbf{b}^\top \mathbf{y}|}{\max\{1, \min\{|\mathbf{c}^\top \mathbf{x}|, |\mathbf{b}^\top \mathbf{y}|\}\}} \leq \varepsilon_{\text{rel}}. \end{aligned}$$

Since CuClarabel also uses an interior-point method, all iterates of CuClarabel are within the cones.

References

- [1] David Applegate, Mateo Díaz, Oliver Hinder, Haihao Lu, Miles Lubin, Brendan O’Donoghue, and Warren Schudy. Practical large-scale linear programming using primal-dual hybrid gradient. In *Advances in Neural Information Processing Systems*, volume 34, pages 20243–20257, 2021.
- [2] David Applegate, Oliver Hinder, Haihao Lu, and Miles Lubin. Faster first-order primal-dual methods for linear programming using restarts and sharpness. *Mathematical Programming*, 201(1):133–184, 2023.

- [3] MOSEK ApS. MOSEK Modeling Cookbook, 2024. <https://docs.mosek.com/MOSEKModelingCookbook-a4paper.pdf>. Accessed: 2025-04-11.
- [4] Chaithanya Bandi, Nikolaos Trichakis, and Phebe Vayanos. Robust multiclass queuing theory for wait time estimation in resource allocation systems. *Management Science*, 65(1):152–187, 2019.
- [5] Nathan Bell and Michael Garland. Efficient sparse matrix-vector multiplication on CUDA. Technical report, NVIDIA Technical Report NVR-2008-004, NVIDIA Corporation, 2008.
- [6] Alexandre Belloni and Robert M Freund. On the second-order feasibility cone: Primal-dual representation and efficient projection. *SIAM Journal on Optimization*, 19(3):1073–1092, 2008.
- [7] Alexander Biele and Dinakar Gade. FICO® Xpress solver 9.4, 2024. <https://community.fico.com/s/blog-post/a5QQi0000019II5MAM/fico4824>. Accessed: 2025-04-11.
- [8] Edward H Bowman. Production scheduling by the transportation method of linear programming. *Operations Research*, 4(1):100–103, 1956.
- [9] Stephen Boyd, Enzo Busseti, Steven Diamond, Ron Kahn, Peter Nystrup, and Jan Speth. Multi-period trading via convex optimization. *Foundations and Trends in Optimization*, 3(1):1–76, 2017.
- [10] Antonin Chambolle and Thomas Pock. A first-order primal-dual algorithm for convex problems with applications to imaging. *Journal of Mathematical Imaging and Vision*, 40:120–145, 2011.
- [11] Abraham Charnes and William W Cooper. The stepping stone method of explaining linear programming calculations in transportation problems. *Management Science*, 1(1):49–69, 1954.
- [12] Kaihuang Chen, Defeng Sun, Yancheng Yuan, Guojun Zhang, and Xinyuan Zhao. HPR-LP: An implementation of an HPR method for solving linear programming. *arXiv preprint arXiv:2408.12179*, 2024.
- [13] Li Chen, Long He, and Yangfang Zhou. An exponential cone programming approach for managing electric vehicle charging. *Operations Research*, 72(5):2215–2240, 2024.
- [14] Yuwen Chen, Danny Tse, Parth Nobel, Paul Goulart, and Stephen Boyd. CuClarabel: GPU acceleration for a conic optimization solver. *arXiv preprint arXiv:2412.19027*, 2024, 2024.
- [15] Thomas H Cormen, Charles E Leiserson, Ronald L Rivest, and Clifford Stein. *Introduction to algorithms*. MIT Press, 4th edition, 2022.
- [16] NVIDIA Corporation. NVIDIA cuDSS, 2025. <https://developer.NVIDIA.com/cudss>. Accessed: 2025-04-11.

- [17] Qi Deng, Qing Feng, Wenzhi Gao, Dongdong Ge, Bo Jiang, Yuntian Jiang, Jingsong Liu, Tianhao Liu, Chenyu Xue, Yinyu Ye, and Chuwen Zhang. An enhanced alternating direction method of multipliers-based interior point method for linear and conic optimization. *INFORMS Journal on Computing*, 37(2):338–359, 2025.
- [18] Edmund Eisenberg and David Gale. Consensus of subjective probabilities: The pari-mutuel method. *The Annals of Mathematical Statistics*, 30(1):165–168, 1959.
- [19] Ernie Esser, Xiaoqun Zhang, and Tony F Chan. A general framework for a class of first order primal-dual algorithms for convex optimization in imaging science. *SIAM Journal on Imaging Sciences*, 3(4):1015–1046, 2010.
- [20] Alex Fender. Advances in optimization AI, 2024. <https://resources.NVIDIA.com/en-us-ai-optimization-content/gtc24-s62495>. Accessed: 2025-04-11.
- [21] Henrik A Friberg. CBLIB 2014: A benchmark library for conic mixed-integer and continuous optimization. *Mathematical Programming Computation*, 8:191–214, 2016.
- [22] Henrik A Friberg. Projection onto the exponential cone: A univariate root-finding problem. *Optimization Methods and Software*, 38(3):457–473, 2023.
- [23] Dongdong Ge, Haodong Hu, Qi Huangfu, Jinsong Liu, Tianhao Liu, Haihao Lu, Jinwen Yang, Yinyu Ye, and Chuwen Zhang. cuPDL-C, 2024. <https://github.com/COPT-Public/cuPDL-C>. Accessed: 2025-04-11.
- [24] Dongdong Ge, Qi Huangfu, Zizhuo Wang, Jian Wu, and Yinyu Ye. Cardinal Optimizer (COPT) user guide. *arXiv preprint arXiv:2208.14314*, 2022.
- [25] Gregory Glockner. Parallel and distributed optimization with Gurobi, 2023. Accessed: 2025-03-12.
- [26] William H Greene. *Econometric analysis*. Pearson, 7th edition, 2017.
- [27] Richard C. Grinold and Ronald N. Kahn. *Active Portfolio Management: A Quantitative Approach for Producing Superior Returns and Controlling Risk*. McGraw Hill, 2nd edition, 1999.
- [28] Benjamin Halpern. Fixed points of nonexpanding maps. *Bulletin of the American Mathematical Society*, 73(6):957–961, 1967.
- [29] Qiushi Han, Chenxi Li, Zhenwei Lin, Caihua Chen, Qi Deng, Dongdong Ge, Huikang Liu, and Yinyu Ye. A low-rank ADMM splitting approach for semidefinite programming. *arXiv preprint arXiv:2403.09133*, 2024.
- [30] Qiushi Han, Zhenwei Lin, Hanwen Liu, Caihua Chen, Qi Deng, Dongdong Ge, and Yinyu Ye. Accelerating low-rank factorization-based semidefinite programming algorithms on GPU. *arXiv preprint arXiv:2407.15049*, 2024.

- [31] Fred Hanssman and Sidney W Hess. A linear programming approach to production and employment scheduling. *Management Science*, 1(1):46–51, 1960.
- [32] Oliver Hinder. Worst-case analysis of restarted primal-dual hybrid gradient on totally unimodular linear programs. *Operations Research Letters*, 57:107199, 2024.
- [33] Michael Ho, Zheng Sun, and Jack Xin. Weighted elastic net penalized mean-variance portfolio design and computation. *SIAM Journal on Financial Mathematics*, 6(1):1220–1244, 2015.
- [34] Yicheng Huang, Wanyu Zhang, Hongpei Li, Weihai Xue, Dongdong Ge, Huikang Liu, and Yinyu Ye. Restarted primal-dual hybrid conjugate gradient method for large-scale quadratic programming. *arXiv preprint arXiv:2405.16160*, 2024.
- [35] Duan Li and Wan-Lung Ng. Optimal dynamic portfolio selection: Multiperiod mean-variance formulation. *Mathematical finance*, 10(3):387–406, 2000.
- [36] Jiahua Li. Sparse and stable portfolio selection with parameter uncertainty. *Journal of Business & Economic Statistics*, 33(3):381–392, 2015.
- [37] Felix Lieder. On the convergence rate of the Halpern-iteration. *Optimization Letters*, 15(2):405–418, 2021.
- [38] Tianyi Lin, Shiqian Ma, Yinyu Ye, and Shuzhong Zhang. An ADMM-based interior-point method for large-scale linear programming. *Optimization Methods and Software*, 36(2-3):389–424, 2021.
- [39] Haihao Lu and Jinwen Yang. On the infimal sub-differential size of primal-dual hybrid gradient method and beyond. *arXiv preprint arXiv:2206.12061*, 2022.
- [40] Haihao Lu and Jinwen Yang. cuPDLP. jl: A GPU implementation of restarted primal-dual hybrid gradient for linear programming in Julia. *arXiv preprint arXiv:2311.12180*, 2023.
- [41] Haihao Lu and Jinwen Yang. A practical and optimal first-order method for large-scale convex quadratic programming. *arXiv preprint arXiv:2311.07710*, 2023.
- [42] Haihao Lu and Jinwen Yang. On the geometry and refined rate of primal–dual hybrid gradient for linear programming. *Mathematical Programming*, pages 1–39, 2024.
- [43] Haihao Lu and Jinwen Yang. Restarted Halpern PDHG for Linear Programming. *arXiv preprint arXiv:2407.16144*, 2024.
- [44] Haihao Lu, Jinwen Yang, Haodong Hu, Qi Huangfu, Jinsong Liu, Tianhao Liu, Yinyu Ye, Chuwen Zhang, and Dongdong Ge. cuPDLP-C: A strengthened implementation of cuPDLP for linear programming by C language. *arXiv preprint arXiv:2312.14832*, 2023.
- [45] Ho-Yin Mak, Ying Rong, and Jiawei Zhang. Appointment scheduling with limited distributional information. *Management Science*, 61(2):316–334, 2015.

- [46] Hans D Mittelmann. Benchmarks for Optimization Software, 2025. "<https://plato.asu.edu/>". Accessed: 2025-04-12.
- [47] Jean Jacques Moreau. Décomposition orthogonale d'un espace Hilbertien selon deux cônes mutuellement polaires. *Comptes rendus hebdomadaires des séances de l'Académie des sciences*, 255:238–240, 1962.
- [48] Brendan O'Donoghue. Operator splitting for a homogeneous embedding of the linear complementarity problem. *SIAM Journal on Optimization*, 31(3):1999–2023, 2021.
- [49] Brendan O'donoghue, Eric Chu, Neal Parikh, and Stephen Boyd. Conic optimization via operator splitting and homogeneous self-dual embedding. *Journal of Optimization Theory and Applications*, 169:1042–1068, 2016.
- [50] Thomas Pock, Daniel Cremers, Horst Bischof, and Antonin Chambolle. An algorithm for minimizing the Mumford–Shah functional. In *Proceedings of the 2009 International Conference on Computer Vision*, pages 1133–1140. IEEE, 2009.
- [51] Edward Rothberg. New options for solving giant LPs, 2024. <https://www.gurobi.com/events/new-options-for-solving-giant-lps/>. Accessed: 2024-04-11.
- [52] Daniel Ruiz. A scaling algorithm to equilibrate both rows and columns norms in matrices. Technical report, CM-P00040415, 2001.
- [53] Napat Rujeerapaiboon, Daniel Kuhn, and Wolfram Wiesemann. Robust growth-optimal portfolios. *Management Science*, 62(7):2090–2109, 2016.
- [54] Ernest K Ryu and Stephen Boyd. Primer on monotone operator methods. *Applied and Computational Mathematics*, 15(1):3–43, 2016.
- [55] Vadim I Shmyrev. An algorithm for finding equilibrium in the linear exchange model with fixed budgets. *Journal of Applied and Industrial Mathematics*, 3:505–518, 2009.
- [56] Kasia Swirydowicz, Eric Darve, Wesley Jones, Jonathan Maack, Shaked Regev, Michael A Saunders, Stephen J Thomas, and Slaven Peles. Linear solvers for power grid optimization problems: A review of GPU-accelerated linear solvers. *Parallel Computing*, 111:102870, 2022.
- [57] Robert Tibshirani. Regression shrinkage and selection via the Lasso. *Journal of the Royal Statistical Society Series B: Statistical Methodology*, 58(1):267–288, 1996.
- [58] Michael Wagner, Jaroslaw Meller, and Ron Elber. Large-scale linear programming techniques for the design of protein folding potentials. *Mathematical Programming*, 101:301–318, 2004.
- [59] Zikai Xiong. Accessible theoretical complexity of the restarted primal-dual hybrid gradient method for linear programs with unique optima. *arXiv preprint arXiv:2410.04043*, 2024.

- [60] Zikai Xiong. High-probability polynomial-time complexity of restarted PDHG for linear programming. *arXiv preprint arXiv:2501.00728*, 2025.
- [61] Zikai Xiong and Robert M Freund. Computational guarantees for restarted PDHG for LP based on “limiting error ratios” and LP sharpness. *arXiv preprint arXiv:2312.14774*, 2023.
- [62] Zikai Xiong and Robert M Freund. On the relation between LP sharpness and limiting error ratio and complexity implications for restarted PDHG. *arXiv preprint arXiv:2312.13773*, 2023.
- [63] Zikai Xiong and Robert M Freund. The role of level-set geometry on the performance of PDHG for conic linear optimization. *arXiv preprint arXiv:2406.01942*, 2024.
- [64] Yinyu Ye. A path to the Arrow–Debreu competitive market equilibrium. *Mathematical Programming*, 111(1):315–348, 2008.
- [65] TaeHo Yoon and Ernest K Ryu. Accelerated minimax algorithms flock together. *SIAM Journal on Optimization*, 35(1):180–209, 2025.